Quantum mechanical and quasi-classical dynamics of coupled quasiparticle-boson systems

R. Steib
Abteilung Theoretische Physik, Universität Ulm, D–89069 Ulm, Germany

J. L. Schoendorff, H. J. Korsch
Fachbereich Physik, Universität Kaiserslautern, D–67653 Kaiserslautern, Germany

P. Reineker
Abteilung Theoretische Physik, Universität Ulm, D–89069 Ulm, Germany

Statistical and dynamical properties of a quasiparticle coupled to polarization vibrations in a dimer model are investigated using a full quantum mechanical approach.

The propagation of the system is described in terms of Bose/spin coherent states and compared to various quasi-classical descriptions of the system.

The spectrum of the energy eigenvalues and the level spacing distributions of the system are calculated and turn out to be almost regular especially in the strong coupling limit.

It is demonstrated that the usual quasi-classical approach to this problem is not quite satisfactory. This is because the quantum fluctuations in the spin variable give rise to strong EPR-correlations (Einstein-Podolsky-Rosen) which hence should be included into a quasi-classical description.

We show that a limited but satisfactory quasi-classical approximation may be given using a suitable integrable reference Hamiltonian.

I. INTRODUCTION

The problem of the transfer of a quasiparticle (or a particle) coupled to vibrational modes has been under strong discussion in recent years. The Davydov model[1–3] leads to a coupled set of Schrödinger equations for the occupation amplitudes of the quasiparticle. The influence of vibronic bath variables on the excitation transfer was studied in the framework of generalized Master equation[4] and stochastic Liouville equation approaches.[5] Eilbeck et al.[6] introduced the *discrete self-trapping equation* (DST) and studied the properties of stationary solutions. For the case of a symmetric dimer, Kenkre and Campbell[7] derived a closed nonlinear equation for the site-occupation probability difference in terms of Jacobian elliptic functions. They demonstrated the existence of a transition from a free to a self-trapped state. Later on this model was extended to include dissipation effects,[8–10] asymmetry[11–15] and several other aspects.[16–22] Recently the role of non-adiabatic couplings and the the role of the Born-Oppenheimer approximation in a stepwise quantization were studied.[23,24]

However, it is still an open question whether such a (spin-1/2) system can be described in a quasi-classical manner at all.[25,26] Furthermore, since the quasi-classical equations show pronounced chaos for strong coupling, it is interesting to ask what happens in the quantum system itself. This has been answered partially for higher ($j \gg 1/2$) spin representations.[27,28] In Ref. 28 it was shown, that in those systems the level spacing distribution tends to the universal one, expected in quantum systems where the classical dynamics shows chaos. However, for a two level system ($j = 1/2$), the quantum dynamics is different although similar structures in classical and quantum Poinaré sections may be identified for intermediate coupling.[29]

Here, we will show that a complementary approach to the usual quasi-classical treatment of the spin/boson model may be more suitable for the spin-1/2 case. In Section II, we present the Hamiltonian describing the system under consideration. The Hamiltonian can be split into a trivial and a non-trivial part, where the non-trivial part contains the coupling between the two subsystems (quasiparticle and vibrational degrees of freedom). The non-trivial part describes a harmonic oscillator coupled to a two-level system and is of a general type, describing various physical situations.[30–33] In Section III A, we investigate the dynamics of the system following the usual quasi-classical description. For strong coupling we find a pronounced chaotic behavior. The eigenvalues of the Hamiltonian and the level spacing distributions are presented in Section III B. Apparently, the eigenvalues behave quite regularly, especially in the strong coupling limit. Thus, we are led to search for the integrable part of the Hamiltonian responsible for this behavior (Section III C), which results in approximate expressions for the eigenvalues and eigenvectors (Section III D). With the results of Section III C we are able to derive new quasi-classical equations, which are not equivalent to the previous ones. Furthermore these equations show that the system behaves regularly in the strong coupling limit (III F). In Section IV, we introduce quasi-probability distributions and coherent states. The dynamical behavior of the system is illustrated by means of Q-functions. Various expectation values of interest are calculated and compared to the results of a pure classical description.

II. MODEL AND BASIC EQUATIONS

We consider the dynamics of a quasiparticle (or a particle, e.g. exciton or electron) in a molecular dimer. The quasiparticle is moving between the two sites of the dimer due to dipole-dipole interaction. The motion of the quasiparticle is coupled to local vibrational modes at the two sites. The total Hamiltonian is specified by

$$H_{\rm tot} = H_{\rm exc} + H_{\rm vib} + H_{\rm int}, \tag{1}$$

where $H_{\rm exc}$, $H_{\rm vib}$ and $H_{\rm int}$ represent the quasiparticle, the vibrational modes and the interaction between the two subsystems, respectively:

$$H_{\rm exc} = \varepsilon_1 A_1^\dagger A_1 + \varepsilon_2 A_2^\dagger A_2 + T\left(A_1^\dagger A_2 + A_2^\dagger A_1\right), \tag{2a}$$

$$H_{\rm vib} = \omega_1 B_1^\dagger B_1 + \omega_2 B_2^\dagger B_2 + \frac{1}{2}(\omega_1+\omega_2), \tag{2b}$$

$$H_{\rm int} = g_1\left(B_1^\dagger + B_1\right) A_1^\dagger A_1 + g_2\left(B_2^\dagger + B_2\right) A_2^\dagger A_2. \tag{2c}$$

$H_{\rm exc}$ describes the excitation of the quasiparticle and its transfer between the two sites. $A_n^\dagger, A_n$ $(n = 1, 2)$ are creation and annihilation operators for the quasiparticle obeying Fermi commutation relations. ε_n is the site energy of the quasiparticle at site n and T is the transfer matrix element (dipole-dipole interaction). Throughout this paper we use $T = -0.5$ in all numerical calculations. The vibrational modes are described by $H_{\rm vib}$, where ω_n are the frequencies of the intramolecular vibrations at site n. $B_n^\dagger, B_n$ are the corresponding boson amplitude operators. The coupling between quasiparticle and vibrational degrees of freedom is specified by the interaction term $H_{\rm int}$, with coupling constants g_n.

In order to simplify our Hamiltonian $H_{\rm tot}$, we assume that there is exactly *one* quasiparticle excited on the dimer:

$$A_1^\dagger A_1 + A_2^\dagger A_2 = 1. \tag{3}$$

Because of Eq. (3), the quasiparticle subsystem has the properties of a spin-1/2 system. Therefore we introduce three spin operators

$$\sigma_x = A_1^\dagger A_2 + A_2^\dagger A_1, \tag{4a}$$

$$\sigma_y = -i\left(A_1^\dagger A_2 - A_2^\dagger A_1\right), \tag{4b}$$

$$\sigma_z = A_1^\dagger A_1 - A_2^\dagger A_2 \tag{4c}$$

instead of the four Fermi operators. The expectation value $\langle\sigma_z\rangle$ corresponds to the occupation difference between the two sites of the dimer. Using Eq. (3), we can show that

$$\sigma_x^2 + \sigma_y^2 + \sigma_z^2 = 1 \tag{5}$$

is an integral of motion and therefore the motion in σ-space (subspace of the quasiparticle) is restricted to the sphere (5), the so called Bloch sphere. It is more convenient to use polar coordinates (ϕ, θ) in the figures instead of expectation values of the spin operators. The spin operators satisfy the commutation relation (j, k, ℓ cyclic)

$$[\sigma_j, \sigma_k]_- = 2i\sigma_\ell.$$

Furthermore, new Boson operators

$$B_1 = b_1\cos\varphi - b_2\sin\varphi, \tag{6a}$$

$$B_2 = b_1\sin\varphi + b_2\cos\varphi \tag{6b}$$

for the vibrational modes are introduced by a Bogoljubov transformation ($\tan\varphi = g_1/g_2$). It should be noticed that in the case of the symmetric dimer ($g_1 = g_2$), we have $\sin\varphi = \cos\varphi = 1/\sqrt{2}$ and therefore the vibrational mode $b_2, b_2^\dagger$ corresponds to the difference of the original coordinates $q_1 - q_2$ (with $q_n = (B_n + B_n^\dagger)/\sqrt{2\omega_n}$).

Substituting Eq. (3)–(6) and $\omega_1 = \omega_2 =: \omega$ in Eq. (1) the total Hamiltonian splits into two parts:

$$H_{\rm tot} = H_1 + H_2,$$

where H_1 represents a displaced harmonic oscillator depending only on the operators b_1 and $b_1^\dagger$. The non-trivial part H_2 contains the second boson mode and the coupling between the quasiparticle and second vibrational mode $(b_2, b_2^\dagger)$. The two parts of the Hamiltonian H_1, H_2 are completely decoupled. Therefore we consider only the non-trivial part H_2. Dropping the index "2" we finally obtain

$$H = -\eta\sigma_z\left(b^\dagger + b\right) + T\sigma_x + \omega\left(b^\dagger b + \frac{1}{2}\right) + \varepsilon\sigma_z + \tau\left(b^\dagger + b\right), \tag{7}$$

with the new parameters

$$\varepsilon = \frac{1}{2}\left(\varepsilon_2 - \varepsilon_1\right), \tag{8a}$$

$$\eta = \sqrt{g_1^2 + g_2^2}, \tag{8b}$$

$$\tau = \frac{1}{2}\frac{g_2^2 - g_1^2}{\sqrt{g_1^2 + g_2^2}}. \tag{8c}$$

The Heisenberg equations for this Hamiltonian read

$$\dot\sigma_x = -2\left(\varepsilon - \sqrt{2\omega}\eta Q\right)\sigma_y, \tag{9a}$$

$$\dot\sigma_y = 2\left(\varepsilon - \sqrt{2\omega}\eta Q\right)\sigma_x - 2T\sigma_z, \tag{9b}$$

$$\dot\sigma_z = 2T\sigma_y, \tag{9c}$$

$$\dot Q = P, \tag{9d}$$

$$\dot P = -\omega^2 Q + \sqrt{2\omega}(\eta\sigma_z - \tau). \tag{9e}$$

III. MIXED QUANTUM-CLASSICAL DYNAMICS AND SPECTRAL STATISTICS

A. First approach to a mixed quantum-classical description

A first step towards an understanding of the dynamical properties of a quantum system is the investigation of its classical counterpart. We will proceed in this direction by replacing the operators $b, b^\dagger$ by the hermitian position and momentum operators Q, P of the harmonic oscillator with frequency ω

$$Q = \frac{1}{\sqrt{2\omega}}\left(b^\dagger + b\right), \; P = i\sqrt{\frac{\omega}{2}}\left(b^\dagger - b\right). \tag{10}$$

Rewritten in terms of these operators, the Hamiltonian (7) reads

$$H = \varepsilon\sigma_z + T\sigma_x + \sqrt{2\omega}Q(\tau - \eta\sigma_z) + \frac{1}{2}\left(P^2 + \omega^2 Q^2\right). \tag{11}$$

In this form, H can be thought of describing a spin σ_x, σ_y, σ_z coupled to an harmonic oscillator Q, P via the interaction term $\sqrt{2\omega}Q(\tau - \eta\sigma_z)$.

One way of assigning a classical interpretation to the quantum motion is to investigate the time dependence of the mean values, thus neglecting all fluctuations and correlations present in the quantum motion. In order to get the best correspondence between the classical and the quantum motion, the initial state should be an almost classical state, i.e. a state which has minimal fluctuations (see Appendix A for further discussions).

As the main assumption in our calculation, we use the initial Bose/spin coherent state

$$|\psi(0)\rangle = |q_0, p_0\rangle \otimes |s_0\rangle, \tag{12}$$

where $|q, p\rangle$ represents a coherent state of the boson part and $|s\rangle$ a state of the two-level system

$$|s\rangle = |\phi, \theta\rangle = \sin(\theta/2)\,|\downarrow\rangle + e^{-i\phi}\cos(\theta/2)\,|\uparrow\rangle. \tag{13}$$

See Appendix A for additional details. The most reasonable approximation for the time propagation is the ansatz

$$|\psi(t)\rangle = e^{i\varphi(t)}|q(t), p(t)\rangle \otimes |s(t)\rangle. \tag{14}$$

This is reasonable only if $|\psi(t)\rangle$ remains factorized and no entanglement (EPR-correlations) will show up, i.e. the initial Bose/spin coherent state should *not* develop as

$$|\psi(t)\rangle = c_1|q_1, p_1\rangle \otimes |\uparrow\rangle + c_2|q_2, p_2\rangle \otimes |\downarrow\rangle$$

where $q_1 \neq q_2$, $p_1 \neq p_2$.

Inserting this ansatz into the *time-dependent variational principle*[34] (TDVP), and performing the variation with respect to the coordinates $q(t)$, $p(t)$ and the spin-part $|s(t)\rangle$, we finally arrive at a classical set of differential equations for the behavior of the expectation values in this approximation (see Appendix B 2 for a detailed derivation):

$$\dot{s}_x = -2\left(\varepsilon - \sqrt{2\omega}\eta q\right)s_y, \tag{15a}$$

$$\dot{s}_y = 2\left(\varepsilon - \sqrt{2\omega}\eta q\right)s_x - 2Ts_z, \tag{15b}$$

$$\dot{s}_z = 2Ts_y, \tag{15c}$$

$$\dot{q} = p, \tag{15d}$$

$$\dot{p} = -\omega^2 q + \sqrt{2\omega}(\eta s_z - \tau). \tag{15e}$$

These equations can also be obtained by simply replacing the operators by c-numbers in the Heisenberg equations (9) according to

$$Q \mapsto q, \; P \mapsto p, \; \sigma_k \mapsto s_k,$$

as well as from the corresponding Hamiltonian.[35] This treatment of the model is often denoted as a mixed quantum-classical description. However we want to stress, that this description neglects the EPR-correlations present in the combined motion (cf. Section III F and Appendix B 1 for a detailed discussion).

A detailed investigation of the system (15) can be found in Ref. 35. Here we give only a brief summary of the relevant results. The dynamics of the system in this approach is found to be both, regular and chaotic. The transition from regular to chaotic behavior depends on the coupling strength η and the total energy

$$E = \varepsilon\sigma_z + T\sigma_x + \sqrt{2\omega}Q(\tau - \eta\sigma_z) + \frac{1}{2}\left(P^2 + \omega^2 Q^2\right) \tag{16}$$

of the system. The behavior can be analyzed by Poincaré sections in both subsystems, quasiparticle and oscillator.

We used a fourth order Runge-Kutta method[36] in connection with a method proposed by Hénon[37] allowing to find the intersections of a trajectory with the surface of section accurately. Despite of the long integration range ($\omega t \approx 10^3$), the relative errors in the two known integrals of motion, namely the energy (16) and the radius of the Bloch sphere (5), turned out to be less than 10^{-7}. In Fig. 1 we show some typical Poincaré sections of the Bloch variables corresponding to the left turning point of the oscillator ($P = 0, \; \dot{P} > 0$).

For small values of the coupling η and low energies, the system shows regular behavior. If the energy exceeds some critical value, a stochastic layer in the vicinity of the symmetric ground state of the quasiparticle appears (Fig. 1 (a)). Increasing the energy further, chaos spreads over large parts of the Bloch sphere, leaving islands of regular behavior in the region of the energetically higher antisymmetric state of the quasiparticle. For stronger coupling, the chaotic behavior already appears at the lowest allowed energies (Fig. 1 (b)). For fixed energy, the

chaotic region grows when the coupling is increased or when the oscillator frequency is decreased.

B. Spectral statistics

In the following, we restrict ourselves to the case of a symmetric dimer ($\varepsilon = \tau = 0$, cf. Eq. (8a) and (8c)). The Hamiltonian of the symmetric dimer

$$H = T\sigma_x - \eta\sigma_z\left(b^\dagger + b\right) + \omega\left(b^\dagger b + \frac{1}{2}\right), \tag{17}$$

is equivalent to the Jaynes-Cummings model[30–32], which is a basic model in quantum optics. The symmetric dimer is invariant under an exchange of the two sites, i.e. the parity operator

$$\mathcal{P} = \sigma_x \exp(i\pi b^\dagger b), \tag{18}$$

commutes with H. The eigenvalues of $\mathcal{P}$ are $p = \pm 1$ (even $\{+\}$ and odd $\{-\}$ parity).

In order to calculate the eigenvalues of the Hamiltonian (17) we expand the wave function $|\psi\rangle$ into the simultaneous eigenvectors of $b^\dagger b$ and σ_z:

$$|\psi\rangle = \sum_{n=0}^{\infty} C_n^{\uparrow}\,|n,\uparrow\rangle + \sum_{n=0}^{\infty} C_n^{\downarrow}\,|n,\downarrow\rangle\,. \tag{19}$$

In the numerical calculations we have to truncate the sums in Eq. (19) at a finite number of terms, say N. Because the eigenvalues with even and odd parity are independent, the calculation of the eigenvalues reduces to the diagonalization of two tridiagonal real $N\times N$ matrices, one for each parity $\{\pm\}$. Plotting the energy spectrum the curves with different parity $\{\pm\}$ intersect, whereas the curves with same parity show avoided level crossings (level repulsion).

For a statistical analysis of the spectrum, we calculate the spectral staircase function (the integrated level density)

$$N(E) = \#\left\{n | E_n < E\right\}, \tag{20}$$

which counts the number of energy levels below the energy E. $N(E)$ can be divided into a smooth part $\bar{N}$ and a fluctuating part N_{fl}. For our system the dominant behavior of the smooth part is a linear function of the energy

$$N_{\mathrm{lin}}(E) = \frac{1}{\omega}E + \text{const.}$$

This is quite reasonable because the term $\omega b^\dagger b$ is the dominant part of the Hamiltonian (17), i.e. the mean level density — averaged over many ($\gtrsim 10$) levels — does not depend on E. A more detailed investigation of the spectral staircase function $N(E)$ shows, that the deviation

$$N(E_n) - N_{\mathrm{lin}}(E_n)$$

from the linear behavior is oscillating quite regularly, as shown in Fig. 2. The frequency of the oscillations depends on E. When studying statistical properties of the spectrum one should take this apparently non-statistical contribution into account in the smooth part $\bar{N}$. Thus we have

$$N(E) = N_{\mathrm{lin}}(E) + N_{\mathrm{osc}}(E) + N_{\mathrm{fl}}(E) \tag{21a}$$
$$= \bar{N}(E) + N_{\mathrm{fl}}(E). \tag{21b}$$

If the smooth part $\bar{N}$ of the staircase function is known, the usual approach is to pass from the set of eigenvalues $\{E_n\}$ to the unfolded spectrum $\{E_n'\}$ using the smooth part $\bar{N}$ of the staircase function:

$$E_n' = \bar{N}(E_n). \tag{22}$$

The unfolded spectrum $\{E_n'\}$ has a mean of unity (the quantities E_n' are dimensionless).

In order to understand this apparently regular behavior of the energy eigenvalues we consider the strong coupling limit analytically. This is done in the following section. The results of both, exact numerical calculation and approximate analytical treatment, are presented in Section III E.

C. The strong coupling limit

In this section, we want to investigate the behavior of the system for strong coupling η, the range where the quasi-classical equations (15) show dominant regions of chaos in phase space. We will show that in the strong coupling limit the system is in fact nearly integrable, in the sense that we can give analytical expressions for eigenvalues and eigenvectors to this Hamiltonian to a reasonable accuracy (see also the derivations in Ref. 38). This will be done by a suitable transformation to a new Hamiltonian (27), which extracts the integrable part of the original Hamiltonian (17). Furthermore the quasi-classical equations (33) coming from this transformed Hamiltonian $\tilde{H}$ show a pronounced regular behavior and the strange level spacing distribution can be reproduced analytically.

For strong coupling η, the dynamics of the system is essentially governed by the combined vibronic/two-level normal mode oscillations originating from the diagonalization of the part

$$H_{\mathrm{vib,int}} = -\eta\sigma_z\left(b^\dagger + b\right) + \omega\left(b^\dagger b + \frac{1}{2}\right) \tag{23}$$

of the Hamiltonian H. Using the unitary transformation

$$\mathcal{U} = \exp\left(\frac{\eta}{\omega}\sigma_z(b^\dagger - b)\right) \tag{24}$$

the part $H_{\mathrm{vib,int}}$ can be put into diagonal form. The transformation $\mathcal{U}(\eta/\omega)$ results in a replacement of the operators according to

$$
\begin{aligned}
b &\rightarrow \mathcal{U}^{-1} b \mathcal{U} &&= b + \tfrac{\eta}{\omega}\sigma_z, \\
b^\dagger &\rightarrow \mathcal{U}^{-1} b^\dagger \mathcal{U} &&= b^\dagger + \tfrac{\eta}{\omega}\sigma_z, \\
\sigma_x &\rightarrow \mathcal{U}^{-1} \sigma_x \mathcal{U} &&= \mathcal{D}\left(-\tfrac{2\eta}{\omega}\right)\sigma^+ + \mathcal{D}\left(\tfrac{2\eta}{\omega}\right)\sigma^-,
\end{aligned}
\tag{25}
$$

where $\sigma^\pm$ represent the spin flip operators

$$
\sigma^+ = \begin{pmatrix} 0 & 1 \\ 0 & 0 \end{pmatrix}, \; \sigma^- = \begin{pmatrix} 0 & 0 \\ 1 & 0 \end{pmatrix}
$$

and $\mathcal{D}(\gamma)$ is the displacement operator[39] (see Appendix A)

$$
\mathcal{D}(\gamma) = e^{\gamma b^\dagger - \gamma^* b}.
$$

Applying the transformations to the Hamiltonian H we get the transformed one $\tilde{H} = \mathcal{U}^{-1} H \mathcal{U}$ as:

$$
\begin{aligned}
\tilde{H} = \omega b^\dagger b + \frac{\omega}{2} - \frac{\eta^2}{\omega} \\
+ T\left[\mathcal{D}\left(-\frac{2\eta}{\omega}\right)\sigma^+ + \mathcal{D}\left(\frac{2\eta}{\omega}\right)\sigma^-\right].
\end{aligned}
\tag{26}
$$

The parity operator (18) remains invariant under the transformation (24), $\mathcal{U}^{-1}\mathcal{P}\mathcal{U} = \mathcal{P}$. Instead of $b, b^\dagger$, we again introduce the operators Q and P (10) of the harmonic oscillator and re-express the Hamiltonian (26) in terms of these operators:

$$
\begin{aligned}
\tilde{H} = \frac{1}{2}\left(P^2 + \omega^2 Q^2\right) - \frac{\eta^2}{\omega} \\
+ \cos(\gamma' P)\sigma_x - \sin(\gamma' P)\sigma_y.
\end{aligned}
\tag{27}
$$

For simplicity of notation, we introduced the abbreviations $\gamma = 2\eta/\omega$ and $\gamma' = \gamma\sqrt{2/\omega}$. This Hamiltonian will be the starting point of a second approach to a mixed quantum-classical description (see Section III F).

D. Approximate calculation of the eigenvalues

As already mentioned above, the transformation $\mathcal{U}$ diagonalizes the part $H_{\mathrm{vib,int}}$ explicitly. The calculation presented below is a kind of perturbative treatment of the remaining part $H_{\mathrm{exc}} = T\sigma_x$, i.e. the approximation is valid for the strong coupling/high energy case.

Calculating the eigenvalues of the transformed Hamiltonian (26), we neglect the contribution of non-diagonal boson matrix elements

$$
\langle n|\, \tilde{H}\, |m\rangle, \; n \neq m.
$$

The diagonal boson matrix elements are

$$
\langle n|\, \tilde{H}\, |n\rangle = \begin{pmatrix} \omega n + \frac{\omega}{2} - \frac{\eta^2}{\omega} & T\langle n|\, \mathcal{D}\left(\frac{2\eta}{\omega}\right)|n\rangle \\ T\langle n|\, \mathcal{D}\left(-\frac{2\eta}{\omega}\right)|n\rangle & \omega n + \frac{\omega}{2} - \frac{\eta^2}{\omega} \end{pmatrix}
$$

and the matrix elements of $\mathcal{D}(\gamma)$ are

$$
\langle n|\, \mathcal{D}(\gamma)\, |n\rangle = e^{-|\gamma|^2/2} \cdot L_n(|\gamma|^2),
$$

where L_n are the Laguerre polynomials.[40] In this approximation the eigenvalues and eigenvectors for even $\{+\}$ and odd $\{-\}$ parity are explicitly given by

$$
\begin{aligned}
\tilde{E}_n^\pm = \omega n + \frac{\omega}{2} - \frac{\eta^2}{\omega} \\
\pm (-1)^n T e^{-\frac{2\eta^2}{\omega^2}} L_n\left(\frac{4\eta^2}{\omega^2}\right).
\end{aligned}
\tag{28}
$$

The corresponding eigenvectors can be written as a superposition

$$
|\psi_n^\pm\rangle = \frac{1}{\sqrt{2}}\Big(|n\rangle \otimes |\uparrow\rangle \pm (-1)^n |n\rangle \otimes |\downarrow\rangle\Big),
\tag{29}
$$

where $|\uparrow\rangle$ and $|\downarrow\rangle$ are eigenstates of σ_z and $|n\rangle$ are eigenstates of $b^\dagger b$. Thus the eigenvectors $|\psi_n^\pm\rangle$ have the following parity:

$$
\mathcal{P}|\psi_n^\pm\rangle = \pm|\psi_n^\pm\rangle.
\tag{30}
$$

The results of the approximate analytical calculation of the eigenvalues (28) and the exact numerical results are presented in the following Section.

E. Results for the spectral statistics

We have used up to 400 000 Fock states in our numerical calculations. In order to avoid non-uniformities at the lower end of the spectrum and truncation effects in the highest levels we used only levels from an intermediate energy range for the statistics. Because of the truncation of the sum (19) in the numerical calculation, it is necessary to check how many levels are reliable. We found that at least the lowest 97% of the eigenvalues calculated with $N = 20\,000 \ldots 200\,000$ states do not show relative deviations of more than 10^{-11} compared with the levels calculated with $N = 400\,000$ states.

In Fig. 3 we compare the eigenvalues $\tilde{E}_n$ (Eq. (28), strong coupling/high energy approximation) to those obtained by the exact numerical diagonalization of the Hamiltonian (17). Evidently the approximation holds for large coupling constants γ. The energy range in Fig. 3 starts with eigenvalue number 100. For higher energies the agreement is better than for smaller energies.

Because only the linear part of the staircase function is known, the spectra were unfolded using this linear part

$$
E'_n = N_{\mathrm{lin}}(E_n).
\tag{31}
$$

The distributions of the level spacings $s_n = E'_{n+1} - E'_n$ of the exact and the approximate calculations are compared in Fig. 4. Obviously. the distributions show no significant differences. Even for small coupling ($\gamma = 1$, Fig. 4 (a)), where the approximation is not too good for the levels, there are only non-significant differences in the

distribution of the spacings. I.e. the level spacing distribution can be explained using the approximate energies (28) coming from the diagonal contribution of the transformed Hamiltonian (26). In particular, the absence of small spacings, that have previously been interpreted as an evidence for quantum chaos[41,23] can be attributed to the integrable part

$$\tilde{H}_0 = \omega b^\dagger b + \frac{\omega}{2} - \frac{\eta^2}{\omega} + Te^{-\frac{2\eta^2}{\omega^2}} L_{b^\dagger b}\left(\frac{4\eta^2}{\omega^2}\right)\sigma_x.$$

of the system (cf. Eq. (28)).

As already mentioned above, one should take the regular oscillations $N_{\rm osc}$ into account in the smooth part $\bar{N}$ of the spectral staircase function. If we consider the eigenvalues coming from the approximate calculation (28) as the regular part of the spectrum, the distribution of the differences $\tilde{s}_n \equiv E_n - \tilde{E}_n$ is Poissonian, which is typical for the level spacing distributions of integrable systems.

F. Second approach to a mixed quantum-classical description

In the same way as for the Hamiltonian (7), we can derive quasi-classical equations of motion for the transformed system $\tilde{H}$:

$$\tilde{H} = \frac{1}{2}\left(P^2 + \omega^2 Q^2\right) - \frac{\eta^2}{\omega} + \cos(\gamma' P)\sigma_x - \sin(\gamma' P)\sigma_y.$$

Like Eq. (7) this Hamiltonian describes a harmonic oscillator coupled to a spin. However, the coupling between the spin and the oscillator is now a parametric-like coupling in which the frequency of the spin motion depends on the oscillator through higher powers of the momentum operator P. We use the same ansatz as in Sect. III A, i.e.

$$|\tilde{\psi}(t)\rangle = |\tilde{q}(t), \tilde{p}(t)\rangle \otimes |\tilde{s}(t)\rangle,$$

where $|\tilde{q}(t), \tilde{p}(t)\rangle$ is a Bose coherent state and $|\tilde{s}(t)\rangle$ a pure quantum state of the spin subsystem. Performing the variation with respect to the coordinates $\tilde{q}(t)$, $\tilde{p}(t)$ and the spin-part $|\tilde{s}(t)\rangle$, we get the following mixed set of equations (see Appendix B 3 for detailed derivations)

$$\dot{\tilde{q}} = \tilde{p} - \gamma' T e^{-\frac{1}{2}|\gamma|^2}\left(\sin(\gamma'\tilde{p})\tilde{s}_x + \cos(\gamma'\tilde{p})\tilde{s}_y\right), \quad (32a)$$

$$\dot{\tilde{p}} = -\omega^2 \tilde{q}, \quad (32b)$$

coupled to the Schrödinger equation for the spin subsystem

$$i\partial_t|\tilde{s}\rangle = Te^{-\frac{1}{2}|\gamma|^2}\left(\cos(\gamma'\tilde{p})\,\sigma_x - \sin(\gamma'\tilde{p})\,\sigma_y\right)|\tilde{s}\rangle. \quad (32c)$$

Passing to the time dependence of the mean values, we get the system

$$\dot{\tilde{s}}_x = -2Te^{-\frac{1}{2}|\gamma|^2}\sin(\gamma'\tilde{p})\,\tilde{s}_z, \quad (33a)$$

$$\dot{\tilde{s}}_y = -2Te^{-\frac{1}{2}|\gamma|^2}\cos(\gamma'\tilde{p})\,\tilde{s}_z, \quad (33b)$$

$$\dot{\tilde{s}}_z = 2Te^{-\frac{1}{2}|\gamma|^2} \times \times\Big\{\sin(\gamma'\tilde{p})\,\tilde{s}_x + \cos(\gamma'\tilde{p})\,\tilde{s}_y\Big\}, \quad (33c)$$

$$\dot{\tilde{q}} = \tilde{p} - \gamma' T e^{-\frac{1}{2}|\gamma|^2} \times \times\Big\{\sin(\gamma'\tilde{p})\,\tilde{s}_x + \cos(\gamma'\tilde{p})\,\tilde{s}_y\Big\}, \quad (33d)$$

$$\dot{\tilde{p}} = -\omega^2\tilde{q}. \quad (33e)$$

If the factor $e^{-\frac{1}{2}|\gamma|^2} = e^{-2\eta^2/\omega^2}$ becomes small (intermediate and strong coupling: $\eta \approx \omega$ and $\eta \gg \omega$), the system is nearly integrable. In this case we get

$$\dot{\tilde{s}}_x \approx 0, \quad \dot{\tilde{s}}_y \approx 0, \quad \dot{\tilde{s}}_z \approx 0, \quad (34a)$$

i.e. the spin will hardly show any motion. For the oscillator we have

$$\dot{\tilde{q}} \approx \tilde{p}, \quad \dot{\tilde{p}} = -\omega^2\tilde{q}. \quad (34b)$$

Thus oscillator and spin are almost decoupled and the system is nearly integrable.

In the small coupling case ($\eta \ll \omega$) the Hamiltonian is almost integrable as well because in this case the two subsystems are nearly decoupled. Thus in both limiting cases, the classical system of $\tilde{H}$ shows regular behavior. Comparing the above equations (33) to the Heisenberg equations for the operators σ_k

$$\dot{\sigma}_x = -2T\sin(\gamma' P)\sigma_z, \quad (35a)$$

$$\dot{\sigma}_y = -2T\cos(\gamma' P)\sigma_z, \quad (35b)$$

$$\dot{\sigma}_z = 2T\left\{\sin(\gamma' P)\sigma_x + \cos(\gamma' P)\sigma_y\right\} \quad (35c)$$

and the operators Q and P

$$\dot{Q} = P - \gamma' T\left\{\sin(\gamma' P)\,\sigma_x + \cos(\gamma' P)\,\sigma_y\right\}, \quad (35d)$$

$$\dot{P} = -\omega^2 Q, \quad (35e)$$

we recognize the same structure. The transfer matrix element T however, is effectively reduced to

$$T \to T\exp\left(-|\gamma|^2/2\right),$$

which is caused by the fluctuations

$$\langle P^n\rangle - \langle P\rangle^n \neq 0$$

in the Boson mode (cf. Appendix A).

IV. QUANTUM MECHANICAL DYNAMICS

A. Time evolution and initial states

In this section we investigate the time evolution of the state vector $|\psi(t)\rangle$ for various initial conditions. The time

propagation has been calculated in the basis of the the simultaneous eigenvectors of $b^\dagger b$ and σ_z as in Eq. (19):

$$|\psi(t)\rangle = \sum_{n=0}^{\infty} C_n^{\uparrow}(t)\,|n,\uparrow\rangle + \sum_{n=0}^{\infty} C_n^{\downarrow}(t)\,|n,\downarrow\rangle\,. \tag{36}$$

In this representation the Schrödinger equation

$$i\frac{\partial}{\partial t}\,|\psi(t)\rangle = H\,|\psi(t)\rangle\,,$$

for the Hamiltonian (7) is equivalent to the set of first order differential equations for the coefficients $C_n^{\uparrow}(t)$ and $C_n^{\downarrow}(t)$:

$$\begin{aligned} i\partial_t C_n^{\uparrow}(t) &= \sum_m H_{n,m}^{\uparrow\uparrow} C_m^{\uparrow}(t) + \sum_m H_{n,m}^{\uparrow\downarrow} C_m^{\downarrow}(t), \\ i\partial_t C_n^{\downarrow}(t) &= \sum_m H_{n,m}^{\downarrow\uparrow} C_m^{\uparrow}(t) + \sum_m H_{n,m}^{\downarrow\downarrow} C_m^{\downarrow}(t), \end{aligned}$$

with the matrix elements

$$\begin{aligned} H_{n,m}^{\uparrow\uparrow} &\equiv \langle n,\uparrow|H|m,\uparrow\rangle, \\ &= (n+1/2)\,\omega\,\delta_{n,m} \\ &\quad -\eta\left(\sqrt{n}\,\delta_{n,m+1} + \sqrt{n+1}\,\delta_{n,m-1}\right), \\ H_{n,m}^{\downarrow\downarrow} &\equiv \langle n,\downarrow|H|m,\downarrow\rangle \\ &= (n+1/2)\,\omega\,\delta_{n,m} \\ &\quad +\eta\left(\sqrt{n}\,\delta_{n,m+1} + \sqrt{n+1}\,\delta_{n,m-1}\right), \\ H_{n,m}^{\uparrow\downarrow} &\equiv \langle n,\uparrow|H|m,\downarrow\rangle = T\,\delta_{n,m}\,, \\ H_{n,m}^{\downarrow\uparrow} &\equiv \langle n,\downarrow|H|m,\uparrow\rangle = T\,\delta_{n,m}\,. \end{aligned}$$

The time evolution has been calculated for certain initial Bose/spin coherent states (cf. Appendix A for notation)

$$|\psi(0)\rangle = |q_0,p_0\rangle \otimes |s_0\rangle\,, \quad s_0 = (\phi_0,\theta_0) \tag{37}$$

i.e. coherent states for both subsystems. The coefficients are given by

$$\begin{aligned} C_n^{\uparrow}(0) &= e^{-\frac{1}{2}|\beta_0|^2}\frac{\beta_0^n}{\sqrt{n!}}\,e^{-i\phi_0}\cos(\theta_0/2), \\ C_n^{\downarrow}(0) &= e^{-\frac{1}{2}|\beta_0|^2}\frac{\beta_0^n}{\sqrt{n!}}\,\sin(\theta_0/2), \end{aligned}$$

with

$$\beta = \sqrt{\frac{\omega}{2}}q + \frac{i}{\sqrt{2\omega}}p\,, \quad \beta^* = \sqrt{\frac{\omega}{2}}q - \frac{i}{\sqrt{2\omega}}p.$$

In order to get a valuable image of the inherent correlations and fluctuations of the quantum motion, we illustrate the dynamical behavior by means of the four Q-functions Q_j, $j = 0,\ldots,3$. The representation in terms of Q-functions proves to be most suitable, because they are build upon coherent states and thus reflect most of the classical dynamics hidden in the quantum motion. For a brief review of some properties of Q-functions cf. Appendix A.

B. Time propagation in the transformed system

The time dependence of a state vector $|\psi(t)\rangle$ governed by the original Hamiltonian H (7) may equivalently be described by a state vector $|\tilde{\psi}(t)\rangle$ governed by the Hamiltonian $\tilde{H}$ (26):

$$|\tilde{\psi}(t)\rangle = \exp(-i\tilde{H}t)|\tilde{\psi}(0)\rangle.$$

The relation between corresponding states

$$\begin{aligned} |\tilde{\psi}(t)\rangle &= \mathcal{U}^{-1}\,|\psi(t)\rangle \\ &= \exp\left(-\frac{\eta}{\omega}\sigma_z(b^\dagger - b)\right)|\psi(t)\rangle \end{aligned}$$

and operators $\tilde{X} = \mathcal{U}X\mathcal{U}^{-1}$ is given via the unitary transformation $\mathcal{U}(\eta/\omega)$. For an initially coherent state

$$\begin{aligned} |\psi_0\rangle &= |q_0,p_0\rangle \otimes |s_0\rangle\,, \\ &= |q_0,p_0\rangle \otimes |(\phi_0,\theta_0)\rangle \end{aligned}$$

we get

$$\begin{aligned} |\tilde{\psi}_0\rangle = e^{-i\phi_0} &\times \\ &\times\Big(\cos(\theta_0/2)\,|q_0-\gamma'/2,p_0\rangle \otimes |\uparrow\rangle \\ &+\sin(\theta_0/2)\,|q_0+\gamma'/2,p_0\rangle \otimes |\downarrow\rangle\Big), \end{aligned} \tag{38}$$

where $\gamma' = (2\eta/\omega)\sqrt{2/\omega}$ as before.

Considering the dynamics of the transformed system (27), it is found from the classical equations (33) that — in the strong coupling limit — the spin-part shows only a minor time dependence, whereas the boson mode performs a simple rotation in its phase space, the (q,p)-plane.

C. Trapped states

Starting with a Bose/spin coherent state polarized in positive σ_z direction

$$|\psi_0\rangle = |q_0,p_0\rangle \otimes |\uparrow\rangle\,, \tag{39}$$

one has to consider the time dependence of the state $|\tilde{\psi}_0\rangle$ where

$$|\tilde{\psi}_0\rangle = |q_0-\gamma'/2,p_0\rangle \otimes |\uparrow\rangle\,. \tag{40}$$

This is obviously a Bose/spin coherent state with $\tilde{q}_0 = q_0 - \gamma'/2$, $\tilde{p}_0 = p_0$. In the transformed system the classical motion shows only a simple time dependence (cf. Eq. (34)). The spin remains almost constant

$$\tilde{s}_i \approx \text{const},$$

whereas the boson part performs a simple rotation in the oscillator phase space:

$$\tilde{q}(t) = \tilde{q}_0 \cos(\omega t) + (\tilde{p}_0/\omega) \sin(\omega t)$$
$$\tilde{p}(t) = \tilde{p}_0 \cos(\omega t) - \omega \tilde{q}_0 \sin(\omega t).$$

The time dependence of $|\tilde{\psi}(t)\rangle$ can now be approximated by the expression

$$|\tilde{\psi}(t)\rangle = e^{i\varphi(t)} \, |\tilde{q}_0, \tilde{p}_0\rangle \otimes |\uparrow\rangle \, .$$

The additional phase $\varphi(t)$ accounts for the time dependence of the quantum phase, see Appendix B. In the original system (applying the transformation $\mathcal{U}$ to the corresponding operators) $q(t)$ and $p(t)$ are explicitly given by

$$q(t) = \gamma'/2 + (q_0 - \gamma'/2) \cos(\omega t) + (p_0/\omega) \sin(\omega t) \, ,$$
$$p(t) = p_0 \cos(\omega t) - \omega (q_0 - \gamma'/2) \sin(\omega t).$$

Hence $|\psi(t)\rangle$ will perform an elliptic motion around the center $q = \gamma'/2$, $p = 0$ where the two major-axis are given by $\Delta q = q_0 - \gamma'/2$ and $\Delta p = p_0$. In particular for the initial state $q_0 = \gamma'/2$ and $p_0 = 0$, the state vector will show no motion and thus will appear to be trapped at this point. Obviously the same arguments will hold for a state polarized in negative σ_z direction:

$$|\psi_0\rangle \; = |q_0, p_0\rangle \otimes |\downarrow\rangle \, .$$

In this case, $|\psi(t)\rangle$ will perform an elliptic motion around the center $q = -\gamma'/2$, $p = 0$ with the two major-axis given by $\Delta q = q_0 + \gamma'/2$ and $\Delta p = p_0$. For the initial state $q_0 = -\gamma'/2$ and $p_0 = 0$ the state vector will appear to be trapped as well. Thus the state vectors

$$\left|\psi^{+}_{\rm tr}\right\rangle \; = \left|q^{+}_{\rm tr} = \gamma'/2, p^{+}_{\rm tr} = 0\right\rangle \otimes |\uparrow\rangle \, ,$$
$$\left|\psi^{-}_{\rm tr}\right\rangle \; = \left|q^{-}_{\rm tr} = -\gamma'/2, p^{-}_{\rm tr} = 0\right\rangle \otimes |\downarrow\rangle$$

will remain almost constant in time. This fits perfectly to the exact quantum treatment calculated numerically using the expansion (36) for the state vector. The infinite sums were truncated at an appropriate number of states N. This number is determined by the dynamical behavior of the system. One has to make sure that the contribution of the states with $n > N$ is negligible by checking the distributions of $|C^{\uparrow}_n(t)|^2$ and $|C^{\downarrow}_n(t)|^2$ which must decrease sufficiently fast for $n \to N$.

D. States starting in the 'vicinity' of a trapped state

For states starting in the 'vicinity' of a trapped state we expect that the spin state remains nearly constant, whereas the oscillator will perform a rotation in the phase space around the center $(q^{+}_{\rm tr}, p^{+}_{\rm tr})$, the location of the trapped state.

In Fig. 5 such a state

$$|\psi_0\rangle = \left|q_0 = \frac{3}{2} q^{+}_{\rm tr}, p_0 = p^{+}_{\rm tr}\right\rangle \otimes |\uparrow\rangle \, ,$$

starting in the 'vicinity' of the trapped one is plotted. The Q-function performs the expected rotation in the phase space of the oscillator. The circle corresponding to the rotation is plotted as a dash-dotted line in the figure. At least the oscillator variables can be described by the classical treatment (see Fig. 6 (a)).

The spin variables show very small oscillations but the behavior of the mean-value of the spin-operator varies smoothly as compared to the fast oscillations of its quasi-classical counterparts (Fig. 6 (b) and (c)).

E. Switching the spin orientation

The next initial state we want to discuss is

$$\left|q_0 = q^{+}_{\rm tr}, p_0 = p^{+}_{\rm tr}\right\rangle \otimes |\downarrow\rangle \, ,$$

i.e. the boson part fits to the trapped state $\left|\psi^{+}_{\rm tr}\right\rangle$, but the state of the spin system is switched from $|\uparrow\rangle$ to $|\downarrow\rangle$. For this state we can — as a simple approximation — assume that it behaves like a state starting near the trapped state $\left|\psi^{-}_{\rm tr}\right\rangle$ and thus performs a rotation around the center $(q^{-}_{\rm tr}, p^{-}_{\rm tr})$. But we have to stress, that it is starting at a considerable distance from the point $(q^{-}_{\rm tr}, p^{-}_{\rm tr})$.

In Fig. 7 we have plotted the time evolution of the Q-function Q_3 for this state. We recognize the largest peak rotating around the center $(q^{-}_{\rm tr}, p^{-}_{\rm tr})$ (dash-dotted circle). The negative values of Q_3 show that this rotating peak is correlated with the spin-state $|\downarrow\rangle$.

The additional small structures, which become more and more enhanced as time goes on, can be addressed to small, but still existing EPR-correlations. Regarding the time evolution of this state it is obvious that the state splits into three coherently superposed packets, which are themselves correlated with different spin-states.

We also perceive that up-to $\omega t = 4$ the quasi-classical and quantum trajectories lie close together. Later in time they drift more and more away from each other. This is due to the contribution of the additional structures. The classical trajectory apparently follows the peak moving outside the dash-dotted circle.

F. Superposition of states

Now we consider as an initial condition a Bose/spin coherent state polarized in the positive σ_x direction:

$$|\psi_0\rangle = |q_0, p_0\rangle \otimes \left(|\uparrow\rangle + |\downarrow\rangle\right)/\sqrt{2} \, .$$

The transformed state can be expressed as a superposition of two states

$$|\tilde{\psi}\rangle = \left(|\tilde{\psi}^{+}_0\rangle + |\tilde{\psi}^{-}_0\rangle\right)/\sqrt{2} \, ,$$

where the two parts are given by

$$|\tilde{\psi}_0^+\rangle = |q_0 - \gamma'/2, p_0\rangle \otimes |\uparrow\rangle\,,$$
$$|\tilde{\psi}_0^-\rangle = |q_0 + \gamma'/2, p_0\rangle \otimes |\downarrow\rangle\,.$$

Obviously $|\tilde{\psi}_0\rangle$ does not represent a simple product state as in Sect. IV C, however it may be interpreted as the superposition of the two orthogonal Bose/spin coherent states $|\tilde{\psi}_0^+\rangle$ and $|\tilde{\psi}_0^-\rangle$ which are nearly dynamically independent.

In Fig. 8, we have illustrated the time evolution of such a state, namely

$$|\psi\rangle \;=\; \left|q_0 = q_{\rm tr}^+, p_0 = p_{\rm tr}^+\right\rangle \otimes \frac{1}{\sqrt{2}}\left(|\uparrow\rangle + |\downarrow\rangle\right).$$

The quantum motion is thus the superposition coming from the nearly independent motion of the two Bose/spin coherent states as discussed in the previous sections. At first we have the trapped state $\left|\psi_0^+\right\rangle$ (see Sect. IV C) which is almost motionless. On the other hand, we have the state discussed in Sect. IV E.

In Fig. 8 both parts can be identified clearly. The values of Q_3 show that the moving peak is correlated with the spin-state $|\downarrow\rangle$ whereas the trapped peak is correlated with the spin-state $|\uparrow\rangle$.

Thus we have strong EPR-correlations realized by two peaks moving in the phase space of the oscillator. The time evolution of the corresponding state shows an extremely non-classical behavior, which can *not* be described by a product ansatz

$$|\psi(t)\rangle \;\neq\; |q(t), p(t)\rangle \otimes |s(t)\rangle\,.$$

Here the quasi-classical and quantum trajectories drift away from each other very early. A quasi-classical description is not possible for such a state.

However, since the overlap between both 'partial-states' is negligible, it is possible to interpret the respective time evolution with the help of two coherently superposed states, if one includes the additional phase coming from the TDVP (see Appendix B 1).

G. Time evolution of the occupation difference

In Fig. 9 the quantum mean values s_z for the different initial states described above are plotted:

$$\begin{aligned}
&\text{(a)} \qquad |\psi_0\rangle \;=\; \left|q_0 = q_{\rm tr}^+, p_0 = p_{\rm tr}^+\right\rangle \otimes |\uparrow\rangle = \left|\psi_{\rm tr}^+\right\rangle\,,\\
&\text{(b)} \qquad |\psi_0\rangle \;=\; \left|q_0 = q_{\rm tr}^+, p_0 = p_{\rm tr}^+\right\rangle \otimes |\downarrow\rangle\,,\\
&\text{(c)} \qquad |\psi_0\rangle \;=\; \left|q_0 = q_{\rm tr}^+, p_0 = p_{\rm tr}^+\right\rangle \otimes \left(|\uparrow\rangle + |\downarrow\rangle\right)/\sqrt{2}.
\end{aligned}$$

First, in Fig. 9 (a) we have the trapped state where the spin is nearly constant as it is expected from the quasi-classical description.

The strange time dependence of s_z in Fig. 9 (b) and (c) cannot be described by the simple product ansatz (14), but may be captured by an improved description including EPR-correlations in the quasi-classical treatment using the TDVP. This will be investigated in a forthcoming paper.

V. CONCLUSIONS

We have investigated the properties of a system described by a harmonic oscillator coupled to a two-level system. This model describes various interesting physical situations, e.g. a quasiparticle coupled to polarization vibrations in a dimer model.

We used an approach complementary to the usual quasi-classical treatment. Identifying an integrable Hamiltonian in the strong coupling case, we found that, especially in the strong coupling limit, the system is nearly integrable in contrast to the pronounced chaotic behavior of the usual quasi-classical description. Although both Hamiltonians considered are equivalent (related by an unitary transformation $\mathcal{U}$), the resulting quasi-classical equations are not!

Furthermore the two sets of quasi-classical equations lead to a qualitatively different behavior. The reason for these discrepancies is that the unitary transformation $\mathcal{U}$ will turn a product state into an entangled state and vice versa. Thus the transition from the quantum description to the quasi-classical approximation depends on the selection of a suitable reference Hamiltonian.

If the entire time evolution given by the Schrödinger equation of an initial product state of coherent states can be expressed as a product state

$$|q(t), p(t)\rangle \otimes |s(t)\rangle \;=\; \exp\left(-i\tilde{H}t\right)|q(0), p(0)\rangle \otimes |s(0)\rangle$$

in course of time, the corresponding quasi-classical equations derived from $\tilde{H}$ are expected to give reasonable results. Therefore the quasi-classical description can only be adequate for certain initial conditions of the system. In a spin-1/2 system however, the quantum fluctuations in the spin variables

$$\sqrt{\langle\sigma^2\rangle - \langle\sigma\rangle^2}$$

are very large (of order $\langle\sigma\rangle$). This leads to strong EPR-correlations, i.e. entangled states are very common. Thus a reasonable description of such systems with inherent large quantum fluctuations and thus strong EPR-correlations should be described by tools, which include both, fluctuations and EPR-correlations, in a straightforward manner. This will lead to more degrees of freedom in the TDVP.

ACKNOWLEDGMENTS

We appreciate valuable discussions with A. Engelmann. Financial support from the Deutsche Forschungsgemeinschaft (DFG) is gratefully acknowledged.

APPENDIX A: COHERENT STATE REPRESENTATION

Many properties of Bose coherent states have been examined first by Glauber.[39,42] For each complex number β the coherent state $|\beta\rangle$ is defined by

$$|\beta\rangle = e^{-\frac{1}{2}|\beta|^2} \sum_{n=0}^{\infty} \frac{\beta^n}{\sqrt{n!}} |n\rangle .$$

Each coherent state can be constructed from the ground state $|0\rangle$ ($b\,|0\rangle = 0$) of the harmonic oscillator

$$|\beta\rangle = \mathcal{D}(\beta)\,|0\rangle = e^{-\frac{1}{2}|\beta|^2} e^{\beta b^\dagger} |0\rangle,$$

using the displacement operator $\mathcal{D}(\beta) = \exp(\beta b^\dagger - \beta^* b)$. Because $|\beta\rangle$ is an eigenstate of the annihilation operator ($b|\beta\rangle = \beta|\beta\rangle$), the expectation values of $b^\dagger$ and b for a coherent state $|\beta\rangle$ are given by

$$\langle\beta|b^\dagger|\beta\rangle = \beta^* , \quad \langle\beta|b|\beta\rangle = \beta.$$

Thus $|\beta\rangle$ may be interpreted as a state with amplitude β. The expectation values of the operators Q and P can be calculated straightforwardly using the definition (10)

$$Q = \frac{1}{\sqrt{2\omega}} \left(b^\dagger + b\right),$$
$$P = i\sqrt{\frac{\omega}{2}} \left(b^\dagger - b\right).$$

Introducing real coordinates by $\beta = \sqrt{\omega/2}q + ip/\sqrt{2\omega}$ and identifying $|\beta\rangle \equiv |q,p\rangle$ we get

$$\begin{aligned} \langle q,p|Q|q,p\rangle &= q, \;\; \langle q,p|Q^2|q,p\rangle = q^2 + \tfrac{\omega}{2}, \\ \langle q,p|P|q,p\rangle &= p, \;\; \langle q,p|P^2|q,p\rangle = p^2 + \tfrac{1}{2\omega}. \end{aligned}$$

Furthermore, since the fluctuations in the Q, P variables are minimal in the sense that the uncertainty inequality is an equality

$$\Delta Q\, \Delta P = \frac{1}{2} \tag{A1}$$

for these states, they are close to a prescription of a classical amplitude $\beta = \sqrt{\frac{\omega}{2}}q + \frac{i}{\sqrt{2\omega}}p$.

For various other systems, different from the the harmonic oscillator, similar states have been constructed.[43–45] Following Perelomov[44], we define coherent states

$$|s\rangle = |\phi,\theta\rangle = \sin(\theta/2)\,|\downarrow\rangle + e^{-i\phi}\cos(\theta/2)\,|\uparrow\rangle \tag{A2}$$

for the spin-part. ϕ and θ are polar angles of the phase space of the spin, the sphere. However, in the case of spin-1/2, there is nothing special about these states since a spin-1/2 state is already a coherent state. This is different in the case of higher j-value, e.g. for an N-atom Jaynes-Cummings model. If the quasiparticle is in a coherent state (A2), the expectation values of the spin operators are

$$\begin{aligned} \langle\sigma_x\rangle &= \langle\phi,\theta|\sigma_x|\phi,\theta\rangle = \cos\phi\sin\theta, \\ \langle\sigma_y\rangle &= \langle\phi,\theta|\sigma_y|\phi,\theta\rangle = \sin\phi\sin\theta, \\ \langle\sigma_z\rangle &= \langle\phi,\theta|\sigma_z|\phi,\theta\rangle = \cos\theta. \end{aligned}$$

We illustrate the dynamical behavior of our system by means of the following four Q-functions ($j = 0,\ldots,3$)

$$Q_j(\beta,t) = \mathrm{Tr}\left\{\sigma_j \cdot |\beta\rangle\langle\beta|\,\rho(t)\right\}, \tag{A3}$$

where σ_0 is the identical matrix and

$$\rho(t) = |\Psi(t)\rangle\langle\Psi(t)|$$

is the density operator of the system. Equivalently the functions Q_i can be expressed in terms of the state vector $|\Psi(t)\rangle$ defined by

$$\Psi_\uparrow(\beta,t) = \langle\beta,\uparrow|\Psi(t)\rangle = e^{-\frac{1}{2}|\beta|^2} \sum_{n=0} \frac{(\beta^*)^n}{\sqrt{n!}} C_n^\uparrow(t),$$
$$\Psi_\downarrow(\beta,t) = \langle\beta,\downarrow|\Psi(t)\rangle = e^{-\frac{1}{2}|\beta|^2} \sum_{n=0} \frac{(\beta^*)^n}{\sqrt{n!}} C_n^\downarrow(t).$$

For example, we can express Q_0 and Q_3 as

$$Q_0(\beta,t) = |\Psi_\uparrow(\beta,t)|^2 + |\Psi_\downarrow(\beta,t)|^2 ,$$
$$Q_3(\beta,t) = |\Psi_\uparrow(\beta,t)|^2 - |\Psi_\downarrow(\beta,t)|^2 .$$

From the functions $Q_i(\beta,t)$, we can calculate all moments or expectation values of the state vector $|\Psi\rangle$. Let us first consider the function $Q_0(\beta,t)$, which describes the moments $\langle(b^\dagger)^n b^m\rangle$ of the pure boson mode

$$\begin{aligned} \langle(b^\dagger)^n b^m\rangle &= \mathrm{Tr}\left\{\rho(t)(b^\dagger)^n b^m\right\} \\ &= \int \frac{d^2\beta}{\pi} (\beta^*)^n \beta^m Q_0(\beta,t). \end{aligned}$$

Since $Q_0(\beta,t)$ is the distribution function of the normally ordered moments, the shape of the distribution function $Q_0(\beta,t)$ should reflect the intrinsic fluctuations as well as the 'equal-time' correlations present in the boson mode. Similar properties hold for the other three functions. E.g. we obtain

$$\langle\sigma_z b\rangle = \mathrm{Tr}\{\rho(t)\sigma_z b\} = \int \frac{d^2\beta}{\pi} \beta Q_3(\beta,t).$$

In a similar way, the form of the distribution function Q_i provides an image of the quantum correlation between the spin and the boson mode. The expectation values

$$\langle\sigma_i\rangle = \int \frac{d^2\beta}{\pi} Q_i(\beta,t) \tag{A4}$$

of σ_x, σ_y, σ_z can finally be expressed as integrals over the various Q-functions, where $\langle\sigma_0\rangle = \mathrm{Tr}\{\rho\} = 1$ is the trace of ρ.

APPENDIX B: QUASI-CLASSICAL EQUATIONS

1. The time-dependent variational principle (TDVP)

There are various qualitatively different ways to construct mixed equations of motion where one component of the system is treated classically and the other purely quantum mechanically. The most reasonable approach is to write down the equation of motion for the classical part and the Schrödinger equation for quantum part. The coupling between these two components is approximated by a coupling taking into account only the expectation values of the quantum system. This may be considered as a self-consistent or mean-field approximation to the combined dynamics. However, one should keep in mind that following this procedure certainly neglects the fluctuations present in the nearly classical system. Even more restrictive, also certain EPR-correlations will show up as time goes on.

In order to deal with these aspects in a uniform way we use the *time dependent variational principle*[34] (TDVP) to construct self-consistent equations of motion for mixed quantum-classical systems. This formalism takes the quantum fluctuations, present in the nearly classical system, into account in a straight forward manner. Further this method is — depending on the ansatz — capable to account for EPR-correlations, which might occur in course of time.

The TDVP is based on the simple fact that the stationary points $\psi_c(t)$ of the action functional

$$S[\psi] = \int dt\, \langle\psi(t)|\{-i\partial_t + H\}|\psi(t)\rangle = \int dt\, \mathcal{L} \qquad \text{(B1)}$$

($\langle\psi|\psi\rangle = 1$) are just the solutions of the Schrödinger equation[46]. As a brief example let us consider a harmonic oscillator, the subsystem 1, coupled to a second (quantum) system. The Hamiltonian of the combined system reads

$$H = \frac{1}{2}\left(P^2 + \omega^2 Q^2\right) + H_2 + F_1(Q,P)F_2\,, \qquad \text{(B2)}$$

where F_1 depends only on the operators Q, P of subsystem 1, H_2 is the Hamiltonian of the subsystem 2, and F_2 depends only on operators of subsystem 2.

Assuming that the combined quantum system behaves nearly classical, i.e. the correlation between boson (q,p) and spin (ϕ) degrees of freedom are negligible, we are led to the factorized ansatz

$$\psi(t) = e^{i\varphi(t)}\,|q(t),p(t)\rangle \otimes |\phi(t)\rangle, \qquad \text{(B3)}$$

where $|q(t),p(t)\rangle$ is a coherent state of the oscillator and $|\phi(t)\rangle$ is a state of the second subsystem alone. The reason for inserting the phase $\varphi(t)$ will become clear later. If we plug in this test-function into the TDVP, we get the Lagrangian $\mathcal{L}$

$$\begin{aligned}\mathcal{L} = \dot\varphi + \frac{1}{2}(q\dot p - p\dot q) + \frac{1}{2}\left(p^2+\omega^2q^2\right) + \frac{\omega}{2}\\ +\langle\phi|\{-i\partial_t + H_2\}|\phi\rangle\\ +\langle q,p|F_1(Q,P)|q,p\rangle\langle\phi|F_2|\phi\rangle.\end{aligned}$$

The variation of this Lagrangian with respect to $q(t)$, $p(t)$ and $\phi(t)$ leads to the equations of motion

$$\dot q = p, \qquad \text{(B4a)}$$

$$\dot p = -\omega^2 q - \partial_q \bar F_1(q,p)\,\langle\phi|F_2|\phi\rangle. \qquad \text{(B4b)}$$

$$i\partial_t|\phi\rangle = \{H_2 + \bar F_1(q,p)F_2\}|\phi\rangle, \qquad \text{(B4c)}$$

with $\bar F_1(q,p) = \langle q,p|F_1(Q,P)|q,p\rangle$. Both symbols $\bar F_1$ and F_1 do not coincide in general, unless $F_1(Q,P)$ is a linear function of Q and P.

However, since the phase $\varphi(t)$ enters into the Lagrangian $\mathcal{L}$ only via a total time derivative, φ itself will not appear in the equation of motions. Due to this gauge invariance of the equation of motion with respect the phase φ, it has to be fixed in addition according to

$$\int dt\,\langle\psi(t)|\{-i\partial_t + H\}|\psi(t)\rangle = 0\,, \qquad \text{(B5)}$$

Therefore the phase φ may be omitted in the construction of the quasi-classical equations of motion for this combined subsystem.

2. Equations from the Hamiltonian H

To derive the quasi-classical equations from the Hamiltonian H of the first approach (cf. Eq. 11)

$$\begin{aligned}H = \varepsilon\sigma_z + T\sigma_x + \sqrt{2\omega}Q(\tau - \eta\sigma_z)\\ +\frac{1}{2}\left(P^2+\omega^2Q^2\right)\,,\end{aligned}$$

we use the TDVP ansatz

$$|\psi(t)\rangle = |q(t),p(t)\rangle \otimes |s(t)\rangle, \qquad \text{(B6)}$$

where $|q(t),p(t)\rangle$ is again a coherent state and $|s(t)\rangle$ a pure quantum state of the spin subsystem. Inserting this into the Lagrangian $\mathcal{L}$ we get

$$\begin{aligned}\mathcal{L} = \frac{1}{2}(q\dot p - p\dot q) + \frac{1}{2}\left(p^2+\omega^2q^2\right) + \frac{\omega}{2}\\ +\langle s|\{i\partial_t + \epsilon\sigma_z + T\sigma_x\}|s\rangle\\ +\sqrt{2\omega}\,q\,(\tau - \eta\langle s|\sigma_x|s\rangle).\end{aligned}$$

Performing the variation with respect to the coordinates $q(t)$, $p(t)$ and the spin-part $|s(t)\rangle$ we get the mixed set of equations

$$\dot q = p \quad \dot p = -\sqrt{2\omega}q(\tau - \eta\langle s|\sigma_x|s\rangle)$$

together with the Schrödinger equation for the spin component of the combined system

$$i\partial_t|s\rangle = \{\epsilon\sigma_z + T\sigma_x + \sqrt{2\omega}\, q\,(\tau - \sigma_x)\}|s\rangle.$$

We consider now the time dependence of the various expectation values $s_k = \langle s|\sigma_k|s\rangle$ of the spin subsystem

$$\dot{s}_k = i\langle s(t)|[H_s, \sigma_k]|s(t)\rangle$$

and arrive at a coupled set of differential equations for the approximate behavior of the mean values

$$\dot{s}_x = -2\left(\varepsilon - \sqrt{2\omega}\eta q\right) s_y, \tag{B7a}$$

$$\dot{s}_y = 2\left(\varepsilon - \sqrt{2\omega}\eta q\right) s_x - 2T s_z, \tag{B7b}$$

$$\dot{s}_z = 2T s_y, \tag{B7c}$$

and the oscillator variables

$$\dot{q} = p, \tag{B7d}$$

$$\dot{p} = -\omega^2 q + \sqrt{2\omega}(\eta s_z - \tau). \tag{B7e}$$

It is worthwhile to note, that these equations take the same form as if one calculates the Heisenberg equations and then passes to a classical description by considering all operators as c-numbers. Both prescription coincide here but only because the various operators of the subsystems occur only in linear combinations.

3. Equations from Hamiltonian $\tilde{H}$

To derive the quasi-classical equations for the Hamiltonian

$$\tilde{H} = \frac{1}{2}\left(P^2 + \omega^2 Q^2\right) - \frac{\eta^2}{\omega} + T\cos(\gamma' P)\sigma_x - T\sin(\gamma' P)\sigma_y,$$

of the second approach (cf. Eq. 27), where $\gamma \equiv 2\eta/\omega$ and $\gamma' \equiv \gamma\sqrt{2/\omega}$, we use the same product ansatz (B6) as in the previous section.

Before we can write down the explicit form of the Lagrangian $\mathcal{L}$, we have to evaluate the expectation values of the trigonometric functions $\sin(\gamma' P)$ and $\cos(\gamma' P)$ with respect to a coherent state $|\tilde{q}, \tilde{p}\rangle$. Consider the expectation value $\langle\tilde{q}, \tilde{p}|e^{i\varphi P}|\tilde{q}, \tilde{p}\rangle$. The disentanglement of the exponential operator with the Baker-Campbell-Hausdorff formula leads to

$$e^{i\varphi P} = e^{-\sqrt{\frac{\omega}{2}}(b^\dagger - b)} = e^{-\frac{\omega}{4}\varphi^2} e^{-\sqrt{\frac{\omega}{2}}b^\dagger} e^{\sqrt{\frac{\omega}{2}}b}$$

and the evaluation the expectation value gives

$$\langle\tilde{q}, \tilde{p}|e^{i\varphi P}|\tilde{q}, \tilde{p}\rangle = e^{-\frac{\omega}{2}\varphi^2} e^{i\varphi\tilde{p}}.$$

The Lagrangian becomes

$$\mathcal{L} = \frac{1}{2}\left(\tilde{q}\,\dot{\tilde{p}} - \tilde{p}\,\dot{\tilde{q}}\right) + \frac{1}{2}\left(\tilde{p}^2 + \omega^2\tilde{q}^2\right) + \frac{\omega}{2} - \frac{\eta^2}{\omega} + \langle\tilde{s}| - i\partial_t + Te^{-\frac{1}{2}|\gamma|^2}\left(\cos(\gamma'\tilde{p})\,\sigma_x - \sin(\gamma'\tilde{p})\,\sigma_y\right)|\tilde{s}\rangle.$$

Performing the variation with respect to the coordinates $\tilde{q}(t)$, $\tilde{p}(t)$ and the spin-part $|\tilde{s}(t)\rangle$, we get the following mixed set of equations

$$\dot{\tilde{q}} = \tilde{p} - \gamma' T e^{-\frac{1}{2}|\gamma|^2}\Big\{\sin(\gamma'\tilde{p})\,\tilde{s}_x + \cos(\gamma'\tilde{p})\,\tilde{s}_y\Big\},$$

$$\dot{\tilde{p}} = -\omega^2\tilde{q},$$

coupled to the Schrödinger equation for the spin subsystem

$$i\partial_t|\tilde{s}\rangle = \left\{Te^{-\frac{1}{2}|\gamma|^2}\left(\cos(\gamma'\tilde{p})\,\sigma_x - \sin(\gamma'\tilde{p})\,\sigma_y\right)\right\}|\tilde{s}\rangle.$$

As in the previous section, we consider only the time dependence of the various expectation values $\tilde{s}_k = \langle\tilde{s}|\sigma_k|\tilde{s}\rangle$ of the spin subsystem and which leads to the following set of differential equations:

$$\dot{\tilde{s}}_x = -2Te^{-\frac{1}{2}|\gamma|^2}\sin(\gamma'\tilde{p})\tilde{s}_z.$$

$$\dot{\tilde{s}}_y = -2Te^{-\frac{1}{2}|\gamma|^2}\cos(\gamma'\tilde{p})\tilde{s}_z$$

$$\dot{\tilde{s}}_z = 2Te^{-\frac{1}{2}|\gamma|^2}\Big\{\sin(\gamma'\tilde{p})\tilde{s}_x + \cos(\gamma'\tilde{p})\tilde{s}_y\Big\},$$

$$\dot{\tilde{q}} = \tilde{p} - \gamma' T e^{-\frac{1}{2}|\gamma|^2}\Big\{\sin(\gamma'\tilde{p})\,\tilde{s}_x + \cos(\gamma'\tilde{p})\,\tilde{s}_y\Big\},$$

$$\dot{\tilde{p}} = -\omega^2\tilde{q}.$$

Unlike in the previous section, these equations are not linear in Q and P, which effectively leads to the modification of the transfer matrix element T discussed in Sect. III F.

[1] A. S. Davydov, *Theory of molecular excitations* (Plenum Press, New York, London, 1971).

[2] A. S. Davydov and N. I. Kislukha, phys. stat. sol. (b) **59**, 465 (1973).

[3] A. S. Davydov, J. theor. Biol. **38**, 559 (1973).

[4] V. M. Kenkre, in *Exciton Dynamics in Molecular Crystals and Aggregates*, edited by G. Höhler (Springer-Verlag, Berlin, 1982).

[5] P. Reineker, in *Exciton Dynamics in Molecular Crystals and Aggregates*, edited by G. Höhler (Springer-Verlag, Berlin, 1982).

[6] J. K. Eilbeck, P. S. Lomdahl, and A. C. Scott, Physica D **16**, 318 (1985).

[7] V. M. Kenkre and D. K. Campbell, Phys. Rev. B **34**, 4959 (1986).

[8] V. Szöcs and P. Baňacký, Phys. Rev. A **45**, 5415 (1992).

[9] V. Szöcs, P. Baňacký, and A. Zajac, Phys. Rev. A **45**, 737 (1990).

[10] V. Szöcs, P. Baňacký, and P. Reineker, Chem. Phys. **199**, 1 (1995).

[11] B. Esser and D. Hennig, Z. Phys. B **83**, 285 (1991).

[12] B. Esser and D. Hennig, Phil. Mag. B **65**, 887 (1992).

[13] D. Hennig, Physica Scripta **46**, 14 (1992).

[14] D. Hennig, J. Phys. A **25**, 285 (1992).
[15] D. Hennig and B. Esser, Phys. Rev. A **46**, 4569 (1992).
[16] V. M. Kenkre and G. P. Tsironis, Phys. Rev. B **35**, 1473 (1987).
[17] V. M. Kenkre and H.-L. Wu, Phys. Lett. A **135**, 120 (1989).
[18] V. M. Kenkre and H.-L. Wu, Phys. Rev. B **39**, 6907 (1989).
[19] P. Grigolini, H.-L. Wu, and V. M. Kenkre, Phys. Rev. B **40**, 7045 (1989).
[20] G. P. Tsironis and V. M. Kenkre, Phys. Lett. A **127**, 209 (1989).
[21] G. P. Tsironis, V. M. Kenkre, and D. Finley, Phys. Rev. A **37**, 4474 (1988).
[22] M. I. Salkola, A. R. Bishop, V. M. Kenkre, and S. Raghavan, Phys. Rev. B **52**, R3824 (1995).
[23] H. Schanz and B. Esser, Z. Phys. B **101**, 1299 (1996).
[24] H. Schanz and B. Esser, Phys. Rev. A **55**, 3375 (1997).
[25] R. Graham and M. Höhnerbach, Phys. Lett. **101 A**, 61 (1984).
[26] R. Steib, Diplomarbeit, Universität Ulm, 1995.
[27] M. A. M. de Aguiar, K. Furaya, C. H. Lewenkopf, and M. C. Nemes, Ann. Phys. **216**, 219 (1994).
[28] C. H. Lewenkopf *et al.*, Phys. Lett. A **155**, 113 (1991).
[29] L. Müller, J. Stolze, H. Leschke, and P. Nagel, Phys. Rev. A **44**, 1022 (1991).
[30] E. T. Jaynes and F. W. Cummings, Proc. IEEE **51**, 89 (1963).
[31] M. Tavis and F. W. Cummings, Phys. Rev. **170**, 379 (1968).
[32] M. Tavis and F. W. Cummings, Phys. Rev. **188**, 692 (1969).
[33] H. A. Jahn and E. Teller, Proc. Roy. Soc. **A 161**, 220 (1937).
[34] P. Kramer and M. Saraceno, *Geometry of the Time-Dependent Variational Principle in Quantum Mechanics, Lecture Notes in Physics* **140** (Springer-Verlag, Berlin, Heidelberg, New York, 1981).
[35] B. Esser and H. Schanz, Z. Phys. B **96**, 553 (1995).
[36] W. H. Press, B. P. Flannery, S. A. Teukolsky, and W. T. Vetterling, *Numerical recipes in C* (Cambridge University Press, Cambridge, 1988).
[37] M. Hénon, Physica **5 D**, 412 (1982).
[38] R. Graham and M. Höhnerbach, Z. Phys. B **57**, 233 (1984).
[39] K. E. Cahill and R. J. Glauber, Phys. Rev. **177**, 1857 (1969).
[40] W. Magnus, F. Oberhettinger, and R. P. Soni, *Formulas and theorems for the special functions of mathematical physics* (Springer-Verlag, Berlin, 1966).
[41] M. Cibils, Y. Cuche, and G. Müller, Z. Phys. B **97**, 565 (1995).
[42] R. J. Glauber, Phys. Rev. **131**, 2766 (1963).
[43] W.-M. Zhang, D. H. Feng, and R. Gilmore, Rev. Mod. Phys. **62**, 867 (1990).
[44] A. Perelomov, *Generalized coherent states and their applications* (Springer-Verlag, Berlin, 1986).
[45] J. K. Klauder and B. Skagerstamm, *Coherent States, Applications in Physics and Mathematical Physics* (World Scientific, Singapore, 1985).
[46] P. A. M. Dirac, Proc. Cambridge Philos. Soc. **26**, 376 (1930).

FIG. 1. Poincaré sections for weak ($\gamma = 1,\ \gamma = 2\eta/\omega$) and strong coupling ($\gamma = 4$). In the former case (a) the formation of a stochastic layer in the vicinity of the separatrix can be seen if the energy exceeds a critical value ($E = 3.0$). In the latter case (b) the whole Bloch sphere shows chaotic behavior at this energy. Chaos spreads over large parts of the Bloch sphere already for lower energies (e.g. $E = 0.3$ in (b)). In the upper part of (b) we see remaining regular elliptic islands. The region near $(\phi, \theta) = (\pm\pi, \pi/2)$ is not accessible because the energy ($E = 0.3$) of the system is too low (cf. Eq. (16)).

FIG. 2. Difference between the staircase function $N(E)$ and its dominant (linear) part $N_{\rm lin}$ as a function of n (number of the eigenvalue). As one can easily see, the deviation is oscillating regularly. This non-statistical contribution has to be considered in the smooth part $\bar{N}$ of the staircase function and not in the fluctuation part $N_{\rm fl}$.

FIG. 3. Eigenvalues from an intermediate energy range (levels 100–120). The solid lines show the exact numerical calculations, whereas the dashed lines were calculated using the approximation described in the text. Part (a) presents an overview over a large range of the coupling ($\gamma = 2\eta/\omega$). Evidently the approximation does not hold for small couplings. For higher values of the coupling the approximation is in good agreement with the exact numerical calculations. Part (b) is a magnification of the lower right corner of part (a). The number of Fock states is $N = 800$ and the corresponding eigenfunctions have odd parity.

FIG. 4. Comparison of the level spacing distribution between the exact numerical calculation (solid lines) and the approximation described in the text (dashed lines). Although the approximation is valid only for large coupling strengths and high energies, the approximation leads to good results for the level statistics, even in the case of weak coupling (a). For higher coupling (b) the agreement is even better.

FIG. 5. Time-evolution of quantum vs. quasi-classical description in the oscillator phase space for the initial state $\left|q_0 = \frac{3}{2}q_{\rm tr}^+, p_0 = p_{\rm tr}^+\right\rangle \otimes |\uparrow\rangle$ ($\gamma = 4$). In the l.h.s. of the figure, the solid line represents the quantum trajectory up-to the indicated time ($\omega t = 0.8, 4, 7.2$). The final point of the trajectory is marked by a square. For the quasi-classical description we used a dashed line for the trajectory and a cross for the final point. Additionally the contour-lines of the Q-function $Q_3(t)$ are plotted. The r.h.s. shows the Q-function $Q_3(t)$, where the spin-orientation can be seen. For detailed explanations see the text.

FIG. 6. Quantum expectation values (solid lines) vs. quasi-classical description (dashed lines, resp. dotted lines in (b)) for the oscillator coordinate $q(t)$ and the occupation difference $s_z(t)$ for the same initial state as in Fig. 5. There is no significant difference between quantum and quasi-classical calculation concerning the oscillator variables, whereas the quantum mean-value $s_z(t)$ of the spin-operator varies smoothly as compared to its quasi-classical counterpart.

FIG. 7. The same as Fig. 5 for a different initial state: $\left|q_0 = q_{\rm tr}^+, p_0 = p_{\rm tr}^+\right\rangle \otimes |\downarrow\rangle$.

FIG. 8. The same as in Fig. 5 for a different initial state: $\left|q_0 = q_{\rm tr}^+, p_0 = p_{\rm tr}^+\right\rangle \otimes \frac{1}{\sqrt{2}}(|\uparrow\rangle + |\downarrow\rangle)$.

FIG. 9. Time evolution of the occupation difference $s_z(t)$ (quantum mechanical treatment) for the strong coupling case ($\gamma = 4$). The initial state corresponding to (a) is the trapped state $|\psi_{\rm tr}^+\rangle$. Whereas the initial states for (b) and (c) are the same as in Fig. 7 respectively Fig. 8.

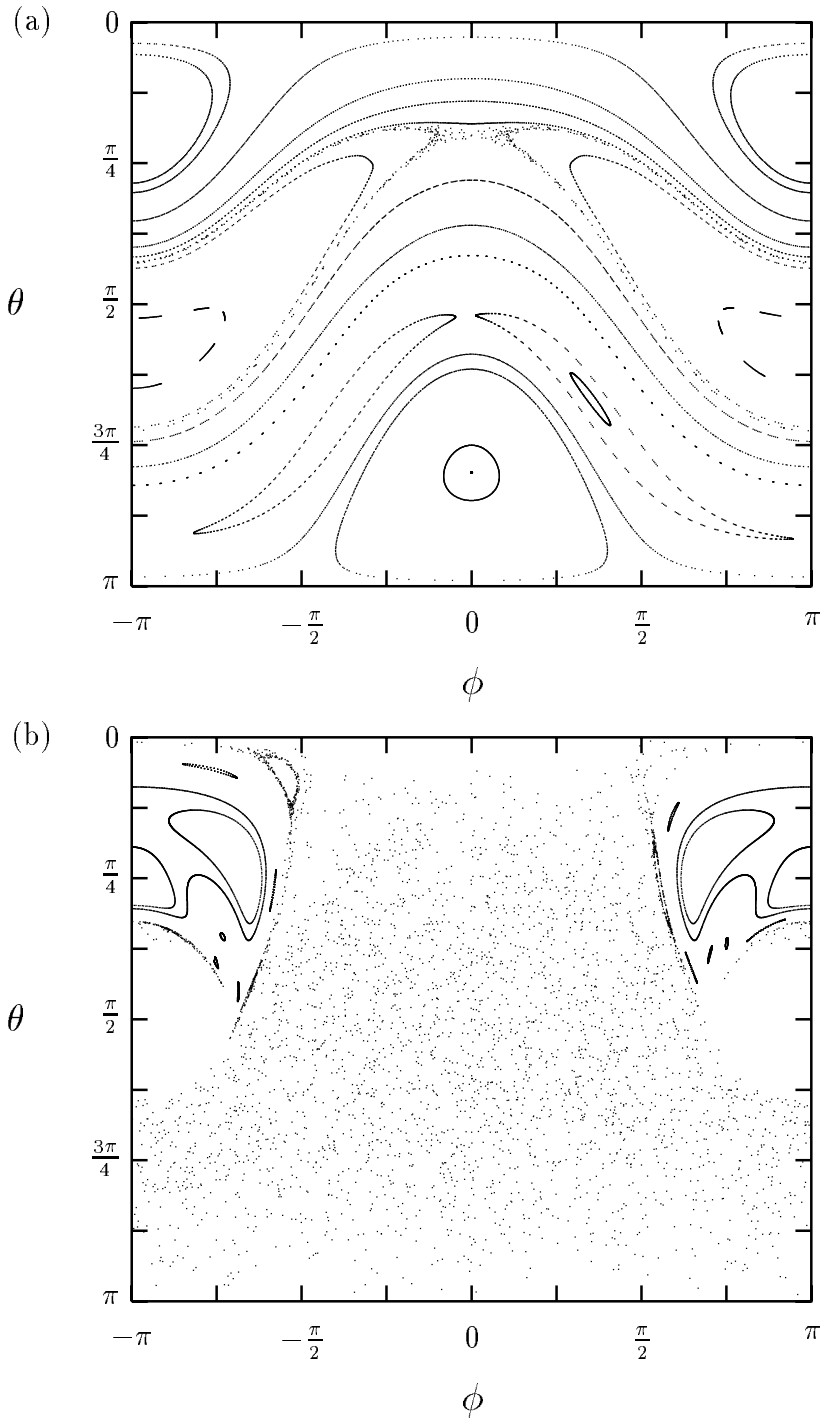

FIG. 1. Poincaré sections for weak ($\gamma = 1,\ \gamma = 2\eta/\omega$) and strong coupling ($\gamma = 4$). In the former case (a) the formation of a stochastic layer in the vicinity of the separatrix can be seen if the energy exceeds a critical value ($E = 3.0$). In the latter case (b) the whole Bloch sphere shows chaotic behavior at this energy. Chaos spreads over large parts of the Bloch sphere already for lower energies (e.g. $E = 0.3$ in (b)). In the upper part of (b) we see remaining regular elliptic islands. The region near $(\phi, \theta) = (\pm\pi, \pi/2)$ is not accessible because the energy ($E = 0.3$) of the system is too low (cf. Eq. (16)).

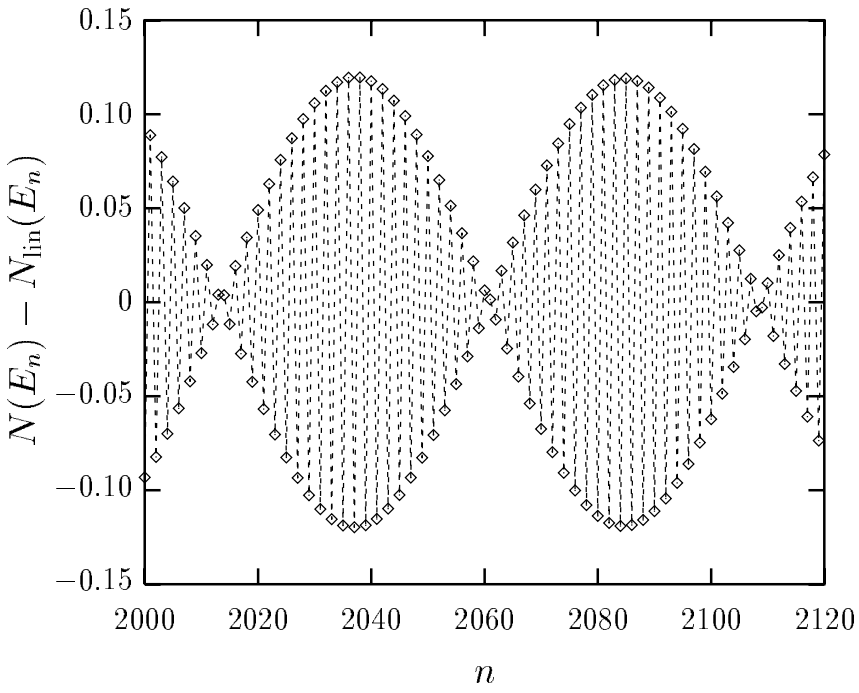

FIG. 2. Difference between the staircase function $N(E)$ and its dominant (linear) part $N_{\rm lin}$ as a function of n (number of the eigenvalue). As one can easily see, the deviation is oscillating regularly. This non-statistical contribution has to be considered in the smooth part $\bar{N}$ of the staircase function and not in the fluctuation part $N_{\rm fl}$.

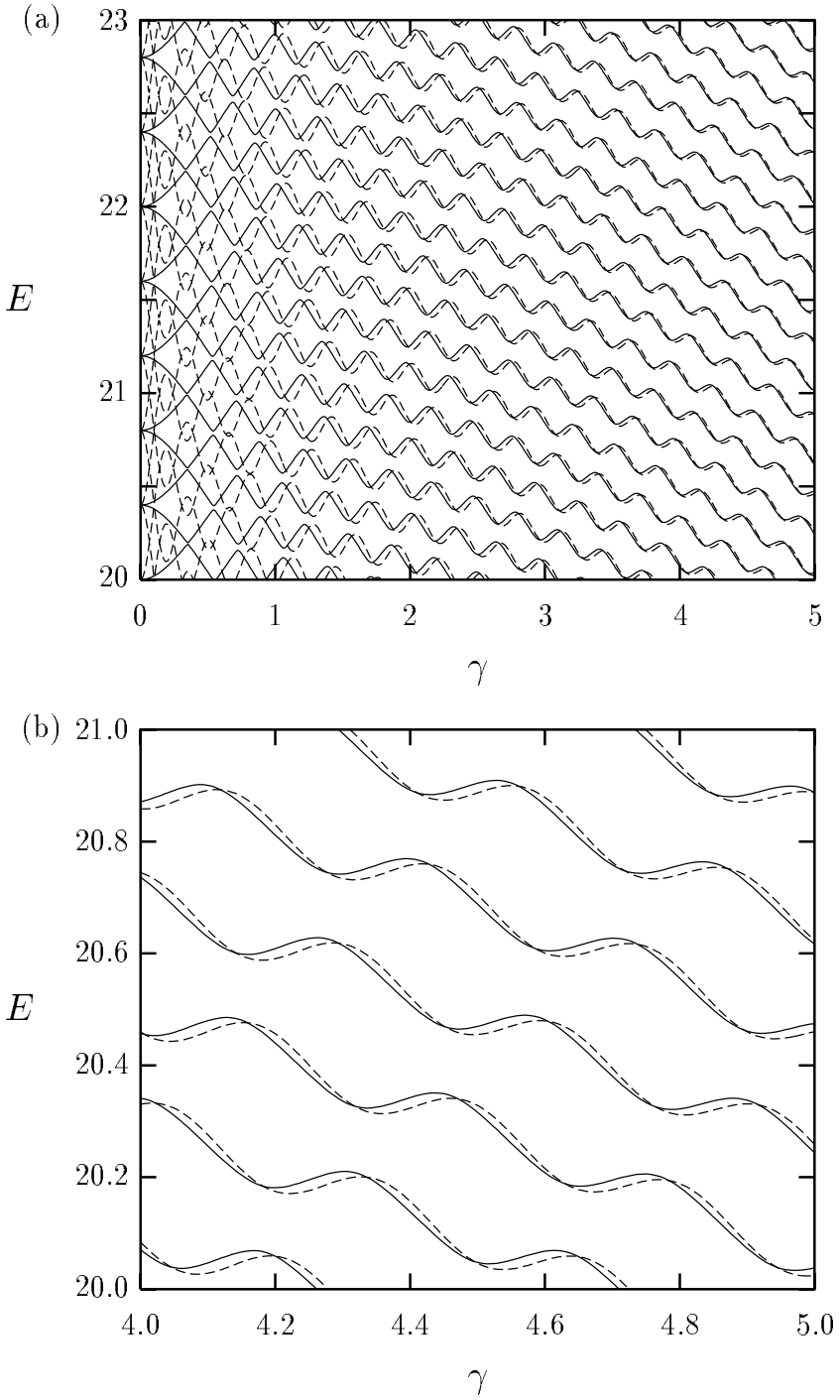

FIG. 3. Eigenvalues from an intermediate energy range (levels 100–120). The solid lines show the exact numerical calculations, whereas the dashed lines were calculated using the approximation described in the text. Part (a) presents an overview over a large range of the coupling ($\gamma = 2\eta/\omega$). Evidently the approximation does not hold for small couplings. For higher values of the coupling the approximation is in good agreement with the exact numerical calculations. Part (b) is a magnification of the lower right corner of part (a). The number of Fock states is $N = 800$ and the corresponding eigenfunctions have odd parity.

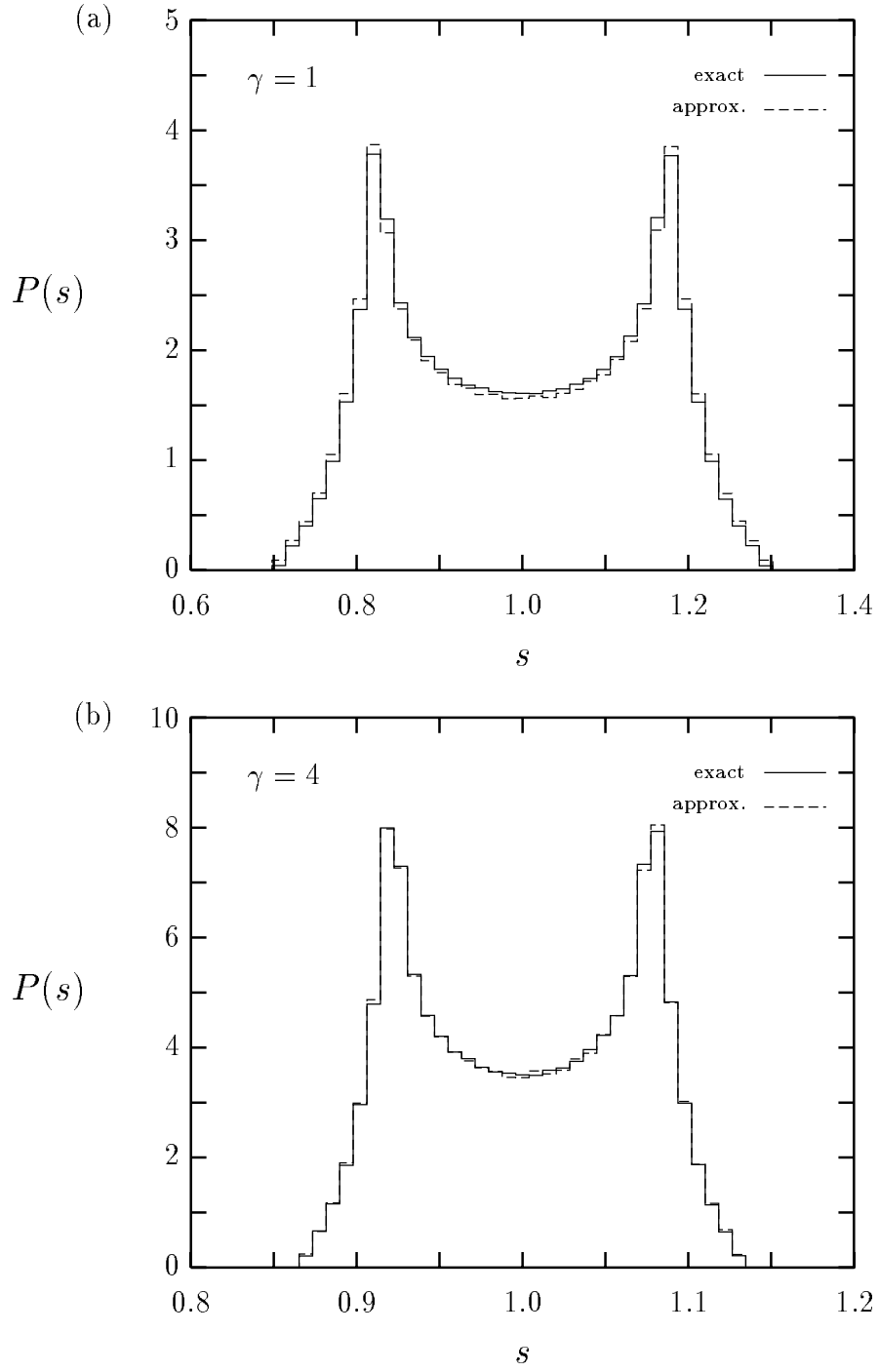

FIG. 4. Comparison of the level spacing distribution between the exact numerical calculation (solid lines) and the approximation described in the text (dashed lines). Although the approximation is valid only for large coupling strengths and high energies, the approximation leads to good results for the level statistics, even in the case of weak coupling (a). For higher coupling (b) the agreement is even better.

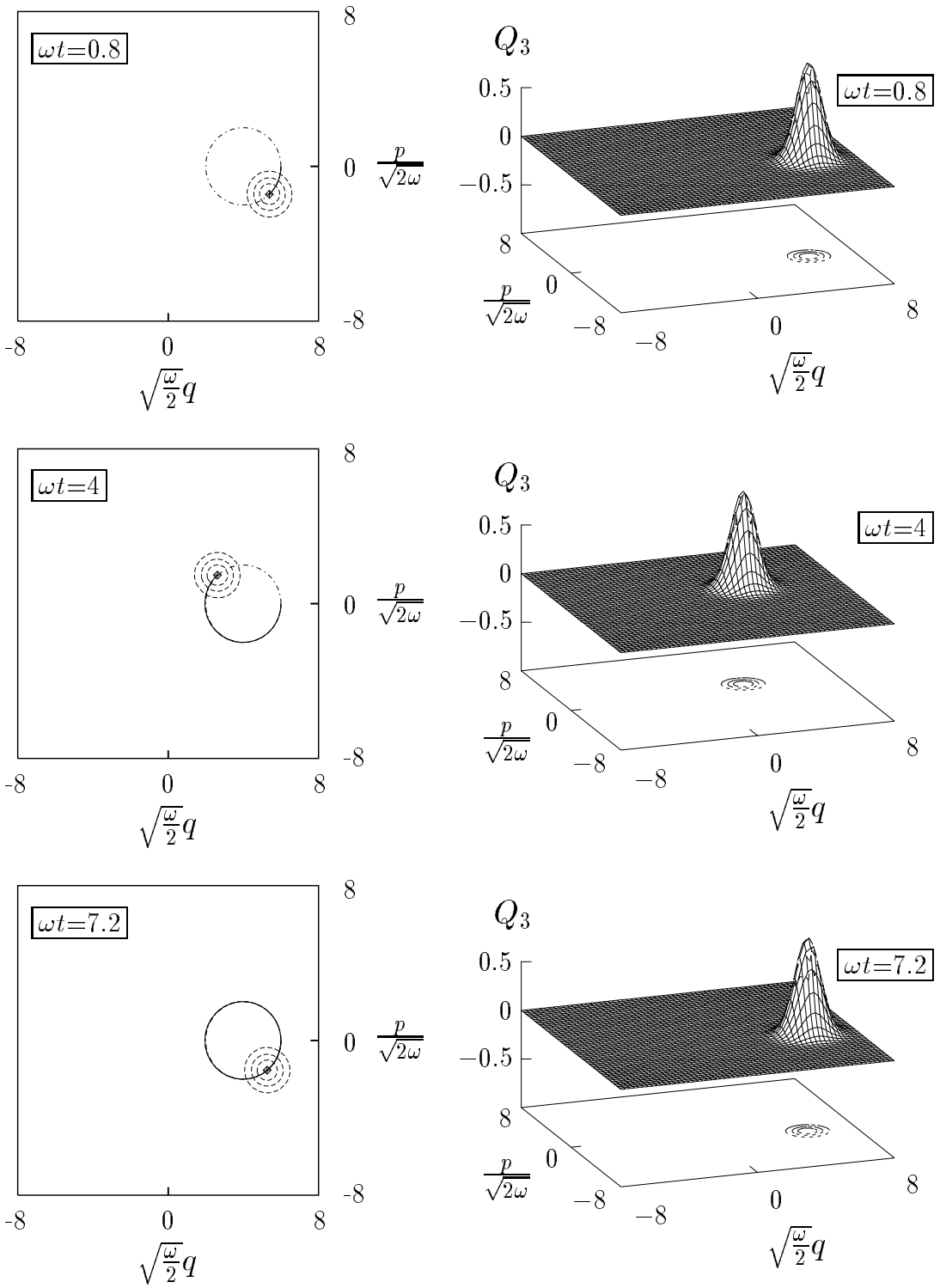

FIG. 5. Time-evolution of quantum vs. quasi-classical description in the oscillator phase space for the initial state $\left|q_0 = \frac{3}{2}q_{\rm tr}^+, p_0 = p_{\rm tr}^+\right\rangle \otimes |\uparrow\rangle$ ($\gamma = 4$). In the l.h.s. of the figure, the solid line represents the quantum trajectory up-to the indicated time ($\omega t = 0.8, 4, 7.2$). The final point of the trajectory is marked by a square. For the quasi-classical description we used a dashed line for the trajectory and a cross for the final point. Additionally the contour-lines of the Q-function $Q_3(t)$ are plotted. The r.h.s. shows the Q-function $Q_3(t)$, where the spin-orientation can be seen. For detailed explanations see the text.

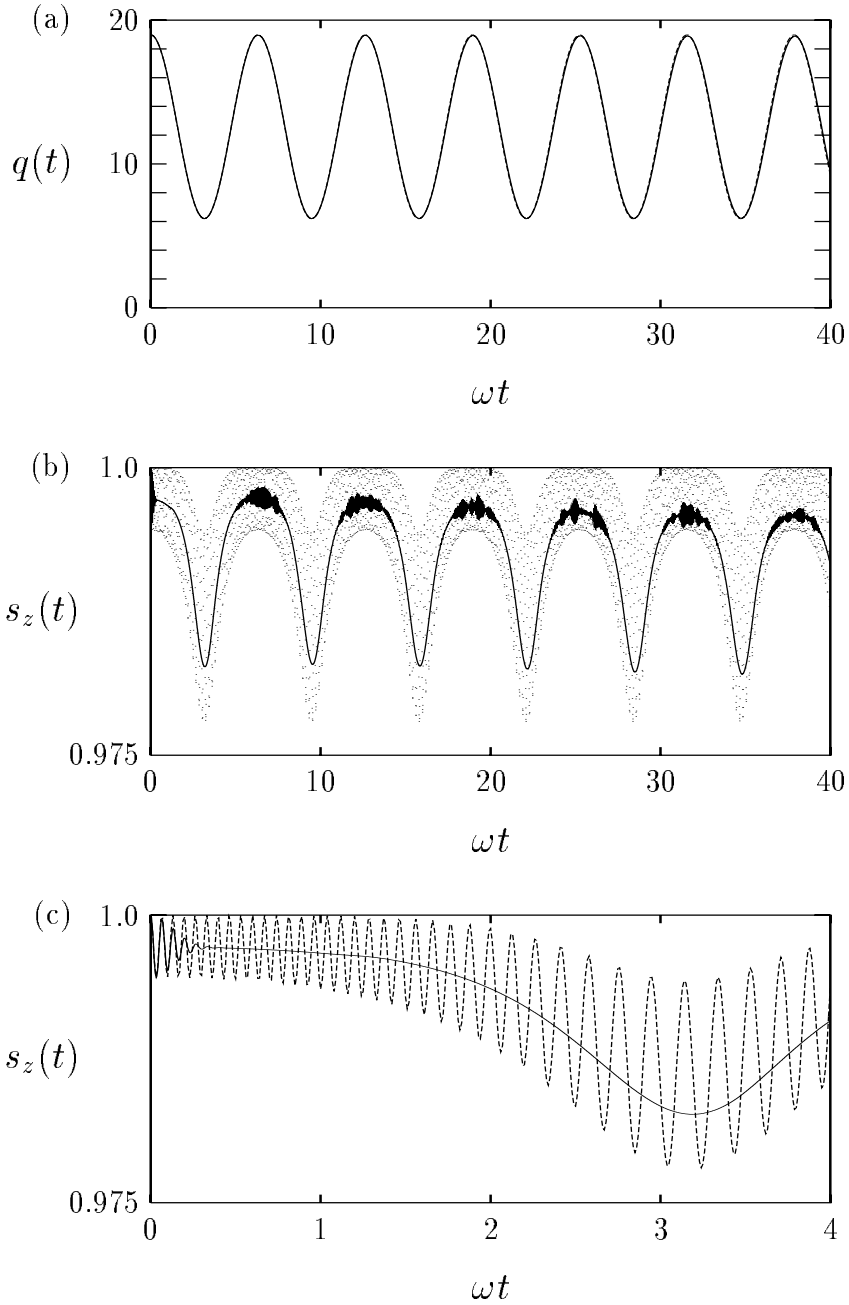

FIG. 6. Quantum expectation values (solid lines) vs. quasi-classical description (dashed lines, resp. dotted lines in (b)) for the oscillator coordinate $q(t)$ and the occupation difference $s_z(t)$ for the same initial state as in Fig. 5. There is no significant difference between quantum and quasi-classical calculation concerning the oscillator variables, whereas the quantum mean-value $s_z(t)$ of the spin-operator varies smoothly as compared to its quasi-classical counterpart.

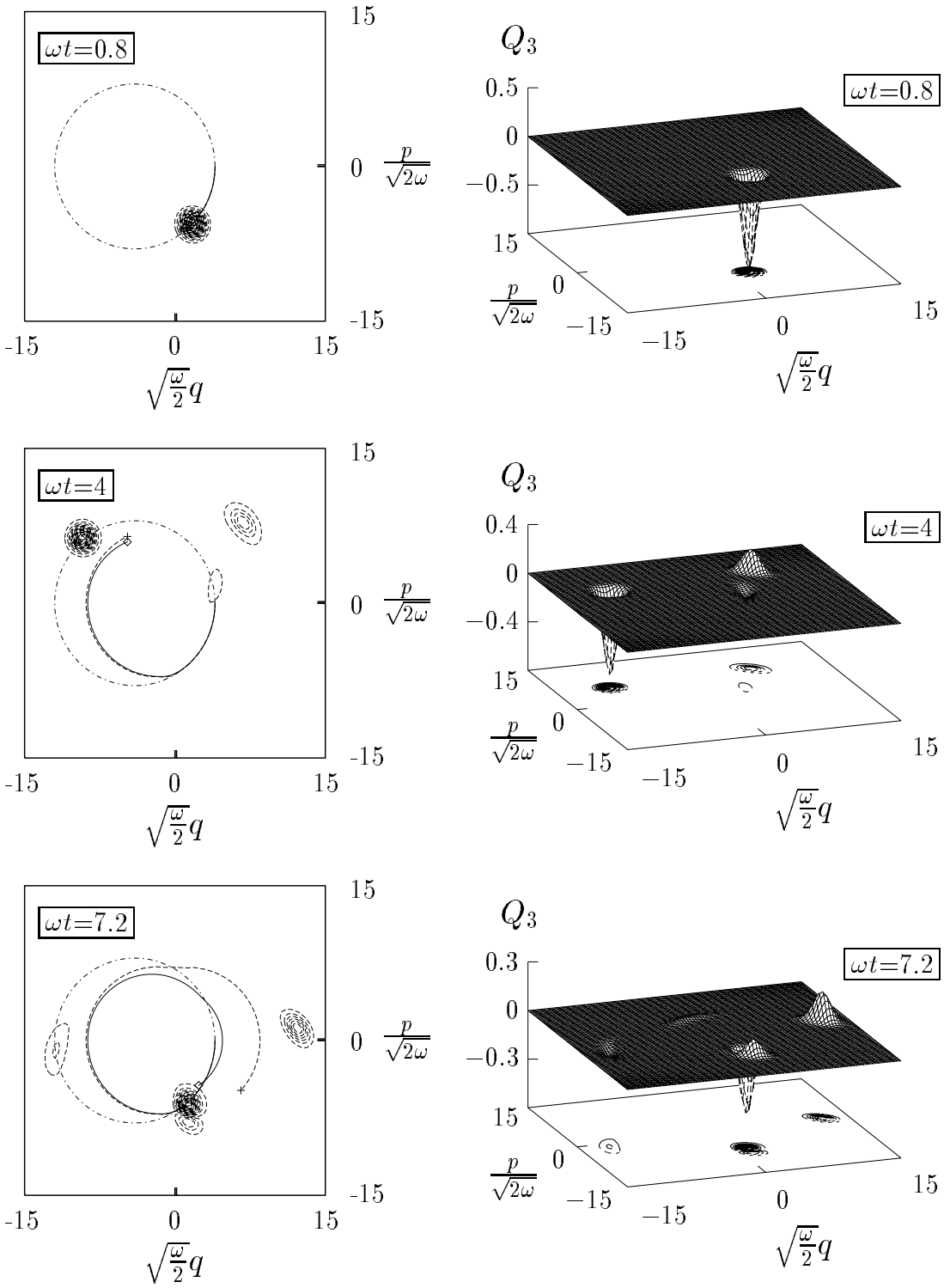

FIG. 7. The same as Fig. 5 for a different initial state: $\left|q_0 = q_{\rm tr}^+, p_0 = p_{\rm tr}^+\right\rangle \otimes |\downarrow\rangle$.

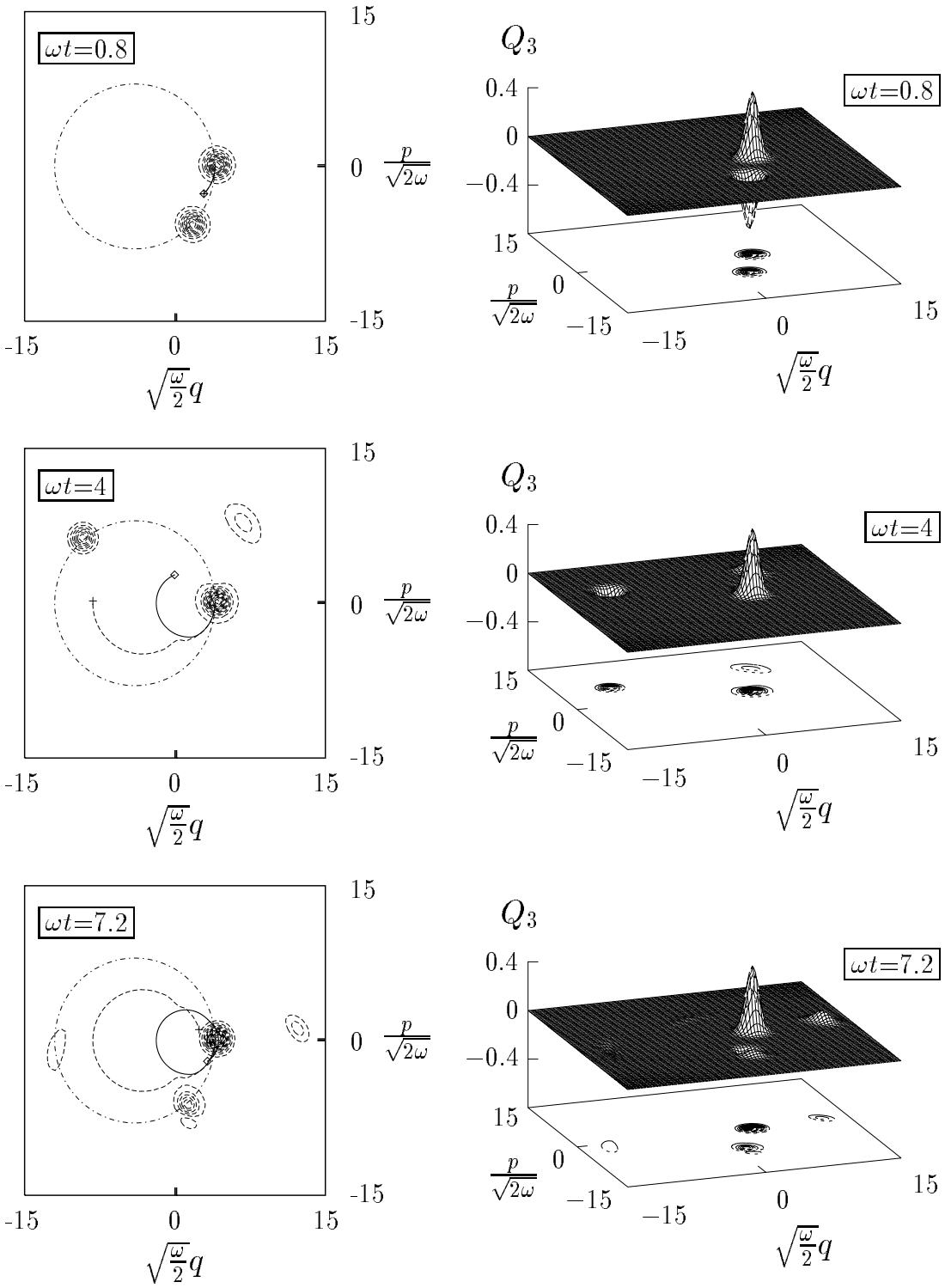

FIG. 8. The same as in Fig. 5 for a different initial state: $\left|q_0 = q_{\rm tr}^+, p_0 = p_{\rm tr}^+\right\rangle \otimes \frac{1}{\sqrt{2}}(|\uparrow\rangle + |\downarrow\rangle)$.

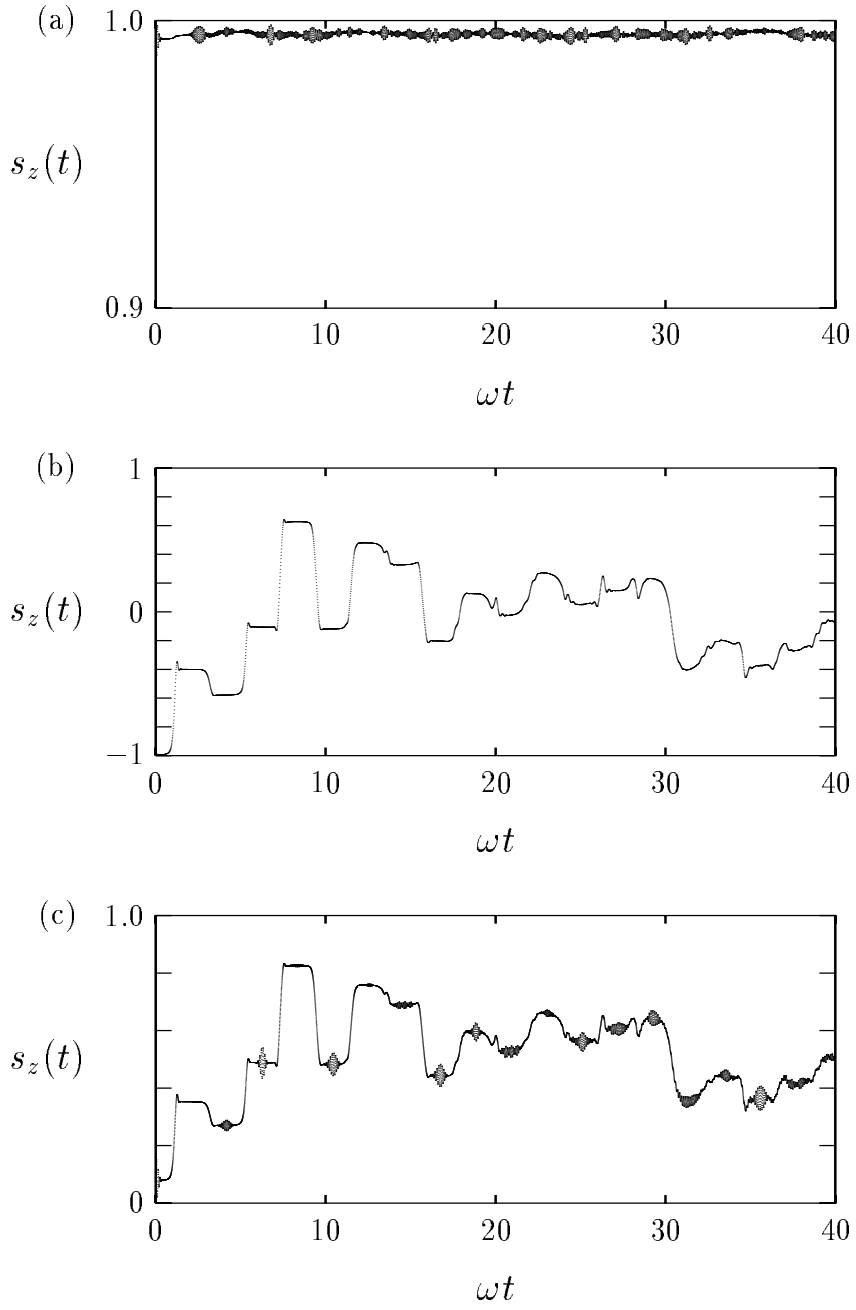

FIG. 9. Time evolution of the occupation difference $s_z(t)$ (quantum mechanical treatment) for the strong coupling case ($\gamma = 4$). The initial state corresponding to (a) is the trapped state $|\psi_{\rm tr}^{+}\rangle$. Whereas the initial states for (b) and (c) are the same as in Fig. 7 respectively Fig. 8.